NASA Contractor Report 3712

An Improved Lambda-Scheme for One-Dimensional Flows

Gino Moretti and Michael T. DiPiano

CONTRACT NAS1-16946
SEPTEMBER 1983

25th Anniversary
1958-1983

NASA

NASA Contractor Report 3712

An Improved Lambda-Scheme for One-Dimensional Flows

Gino Moretti and Michael T. DiPiano
G.M.A.F., Inc.
Freeport, New York

Prepared for
Langley Research Center
under Contract NAS1-16946

NASA
National Aeronautics
and Space Administration

Scientific and Technical
Information Branch

1983

TABLE OF CONTENTS

1. Introduction

Most of the problems in fluid mechanics are multi-dimensional and time-dependent as well. There are few exceptions, which can be expressed using only one time-like variable and one space-like variable. The most important are: spherical and cylindrical time-dependent flows, time-dependent flows in ducts of constant or slightly varying cross-sectional area, and steady, supersonic, two-dimensional or axisymmetric flows. We will generically call them "one-dimensional flows". In this paper, we will focus our attention on those problems where the time-like variable is really time.

What are the reasons for limiting the present analysis to one-dimensional flows? What are the advantages and disadvantages? What is extendable to multi-dimensional flows and what is not? We will begin by outlining some answers to these questions; such answers will guide us in the present study.

The mathematics of one-dimensional problems is much simpler than the mathematics of multi-dimensional problems. From a numerical standpoint, this is reflected in limited storage, simple coding, and the possibility of using a large number of computational nodes. Consequently, numerical tests for accuracy can be conducted by doubling the number of nodes, over and over again. Discontinuities of any kind are perpendicular to the flow, so that their nature is as simple as possible. Finally, there is a certain number of realistic problems for which the exact solution is known. They can be used as benchmarks for a study of accuracy in an absolute fashion. Finally, basic ideas about procedures for accelerating a computation and devices such as multiple grid or multigrid techniques can be also studied.

The main disadvantages of one-dimensional analysis proceed from the unrestricted and uncritical use of the above advantages. The mathematical simplicity of one-dimensional flows, indeed, reflects the physical difference in complexity between one- and multi-dimensional flows. In the latter, waves propagate in more than one direction. One should welcome progress in one-dimensional problems with a guarded optimism towards a better understanding of multi-dimensional problems. Extensions from one-

dimensional ideas and techniques to their multi-dimensional counterparts is far from being a matter of routine. Some methods which have been specifically created for one-dimensional flows may prove to be very difficult to extend to multi-dimensional flows. Methods which require a large number of nodes and whose stepsize is severely limited by the fineness of the mesh may become prohibitive in more than one dimension. Finally, discontinuities in multi-dimensional problems require a knowledge of the orientation of their normal, regardless of the computational technique being used. Nevertheless, jumps across such discontinuities (which obviously occur along the normal to them) can be investigated in a one-dimensional way.

2. Historical background

The goal of numerical calculations of unsteady flows is an accurate description of evolutions of such flows in time (use of unsteady codes to generate steady solutions asymptotically, a device which has been very helpful in the first two decades of electronic computing, is tapering off, for economical reasons). Accuracy implies a detailed description of wave propagation, including various degrees of discontinuities. A proper description of wave propagation relies on defining the domain of dependence of the wave and coding the discretized equations of motion accordingly. The importance of this idea was recognized (but, unfortunately, not emphasized) by Courant, Isaacson and Rees in an early work [1]. Godunov [2] went even farther, by suggesting to consider the local discretization of the Euler equations as the solution of a series of local Riemann problems. For many years, Godunov's suggestion lacked to find developers; some applications [3] oversimplify the original idea, and the accuracy of their two-dimensional applications seems not to be very high.

More recently, integration techniques have been proposed, and are still under development, which emphasize the role of the domain of dependence and which show a proper concern for the analysis of discontinuities. The explicit schemes of Steger [4], Roe [5], van Leer [6] and Osher [7] as well as the λ-scheme [8], all belong to this category. Their importance stems from the possibility of describing complicated multi-dimensional flows,

with transonic effects and an evolving pattern of interacting discontinuities.

The schemes of Steger, Roe, van Leer and Osher all derive from the Euler equations in divergence form. For each one of the equations, the pertinent flux is decomposed in parts which are carried by different waves. The waves are defined by the eigenvectors of the system. For each partial flux, the proper domain of dependence is easily found and the discretization of space derivatives is carried on accordingly. All schemes can be made to have second-order accuracy. Special tests must be performed, and modifications must be made to the standard schemes, to assure monotonicity. Shocks are captured and smeared out over three intervals; contact and gradient discontinuities are also captured and smeared out over an increasing number of intervals as the computation proceeds (we make these statements on the basis of results presented by Pandolfi [9], who uses a variant of Osher's scheme).

The λ-scheme proceeds from the Euler equations written in terms of Riemann parameters and entropy. The definition of domains of dependence is obvious, the coding is extremely simple, and second-order accuracy is easy to achieve. Shocks appears as jumps over a single interval, but they may not move at the right speed or lock in the right position, and they do not provide any jump in entropy, unless special provisions are taken. Contact discontinuities are captured properly and smeared out as in Osher's scheme. Monotonicity at strong gradient discontinuities is not assured.

3. An improved λ-scheme

We intend now to show that very accurate solutions of unsteady, one-dimensional compressible flow problems can be obtained using a coding technique inspired by the λ-scheme, plus adequate tracking of discontinuities. We will show that the handling of discontinuities can be coded, once and for all, essentially using Boolean algebra. The management of the discontinuous features of the flow is, thus, of no concern for the user. In this respect, the computational technique presented in

this paper is equivalent to the other techniques mentioned above [4,5,6,7,9]. We consider our technique more efficient for the following reasons:

1) All discontinuities are captured within one single mesh.

2) The basic integration scheme is much simpler; consequently, it is also faster.

3) The additional logic, related to the presence of discontinuities, is treated in the fastest possible way, through the use of Boolean algebra.

4. Basic equations

We will denote velocity, density, pressure, speed of sound and temperature by u, ρ, p, a, and T, respectively. In a non-dimensional form, $T=p/\rho$, $a^2=\gamma T$. In addition, define $m=\rho u$, $e=p/(\gamma-1)+mu/2$, $h=u(p+e)$, $P=\ln p$, and $s=(P-\gamma \ln \rho)/[\gamma(\gamma-1)]$ (non-dimensional entropy).

The one-dimensional Euler equations in divergence form are

$$v_t + f_x = 0 \tag{1}$$

where

$$v = \begin{bmatrix} \rho \\ m \\ e \end{bmatrix} \quad , \quad f = \begin{bmatrix} m \\ p+mu \\ h \end{bmatrix} \tag{2}$$

Alternatively, the equations can be written in the form

$$w_t + A\, w_x = 0 \tag{3}$$

where

$$w = \begin{bmatrix} P \\ u \\ s \end{bmatrix}, \qquad A = \begin{bmatrix} u & \gamma & 0 \\ a^2/\gamma & u & 0 \\ 0 & 0 & 0 \end{bmatrix} \tag{4}$$

In characteristic form, (3) are written as follows:

$$\begin{aligned} 2P_t + \lambda_1(P_{x1} - \tfrac{\gamma}{a} u_{x1}) + \lambda_2(P_{x2} + \tfrac{\gamma}{a} u_{x2}) &= 0 \\ 2\tfrac{\gamma}{a} u_t - \lambda_1(P_{x1} - \tfrac{\gamma}{a} u_{x1}) + \lambda_2(P_{x2} + \tfrac{\gamma}{a} u_{x2}) &= 0 \\ s_t + u\, s_x &= 0 \end{aligned} \tag{5}$$

where

$$\lambda_1 = u-a, \qquad \lambda_2 = u+a \tag{6}$$

As explained in [8], the subscripts x1, x2 and x all denote x-derivatives. In discretizing (5), however, the derivatives denoted by xi (i=1,2) are approximated by finite differences taken from the side from which λ_i proceeds. The derivative denoted by x alone is approximated by a finite difference taken from the side from which u proceeds.

Riemann invariants can easily be introduced in (5) if the flow is isentropic. In this case, indeed,

$$dP = \frac{\gamma}{\delta} \frac{da}{a} \tag{7}$$

where $\delta = (\gamma-1)/2$ for brevity. Therefore, letting

$$R_1 = \frac{a}{\delta} - u, \qquad R_2 = \frac{a}{\delta} + u \tag{8}$$

the first two equations (5) become:

$$\begin{aligned} \frac{2}{\delta} a_t + \lambda_1 R_{1x1} + \lambda_2 R_{2x2} &= 0 \\ 2 u_t - \lambda_1 R_{1x1} + \lambda_2 R_{2x2} &= 0 \end{aligned} \tag{9}$$

whereas the third equation (5) becomes an identity. If the flow is not isentropic, (7) must be replaced by

$$dP = \frac{\gamma}{\delta}\frac{da}{a} - \gamma\, ds \tag{10}$$

and (9) by

$$\begin{aligned} \frac{2}{\delta}\, a_t - 2as_t + \lambda_1(R_{1x1} - as_{x1}) + \lambda_2(R_{2x2} - as_{x2}) = 0 \\ 2\, u_t - \lambda_1(R_{1x1} - as_{x1}) + \lambda_2(R_{2x2} - as_{x2}) = 0 \\ s_t + u\, s_x = 0 \end{aligned} \tag{11}$$

Note that, to maintain the spirit of (5), in the first two equations (11) the finite differences approximating the derivatives of s are taken in the same direction as the finite differences approximating the derivatives of that R_i to which they are connected. In fact, it is not the domain of dependence of a or s separately which counts, but the domain of dependence of P. The derivative, s_t, in the first equation (11) is obtained from the third equation, where s_x is approximated as specified for (5).

If the flow in a duct of variable cross-section, A=A(x), is considered in a quasi-one-dimensional way, (11) can still be used, provided that a term, $2auA_x/A$ is added to the left-hand side of the first equation.

5. Basic integration scheme

The basic integration scheme for (11) is a variation of the λ-scheme proposed independently by Zhu et al. [10], slightly modified by Pandolfi and Colasurdo (Politecnico di Torino, private communication) and reformulated by the senior author of this paper in a manner which seems easier to extend to multi-dimensional problems [11].

Let

$$f_1 = -\lambda_1(R_{1x1} - a\, s_{x1})$$

$$f_2 = -\lambda_2(R_{2x2} - a\, s_{x2}) \qquad (12)$$

$$f_3 = -u\, s_x$$

$$f_4 = -a\, u\, A_x/A$$

Eqs. (11) can thus be written in the form:

$$a_t = \frac{\delta}{2}(f_1 + f_2 + 2af_3 + 2f_4)$$

$$u_t = \frac{1}{2}(f_2 - f_1) \qquad (13)$$

$$s_t = f_3$$

Let n denote the point to be computed ($x=n\Delta x$) and k the time index ($t=k\Delta t$). Assuming, for argument's sake, that u is positive, f_2, f_3 and f_4 are approximated by

$$f_2 \simeq -\frac{\lambda_{2,n} + \lambda_{2,n-1}}{2}\,\frac{R_{2,n} - R_{2,n-1} - a_n(s_n - s_{n-1})}{\Delta x} \qquad (14)$$

$$f_3 \simeq -\frac{u_n + u_{n-1}}{2}\,\frac{s_n - s_{n-1}}{\Delta x} \qquad (15)$$

$$f_4 \simeq -a_n u_n (A_x/A)_n \qquad (16)$$

and f_1 is approximated by

$$f_1 \simeq -\frac{\lambda_{1,n} + \lambda_{1,n+1}}{2}\,\frac{R_{1,n+1} - R_{1,n} - a_n(s_{n+1} - s_n)}{\Delta x} \qquad (17)$$

if $\lambda_1 < 0$, and by

$$f_1 \simeq -\frac{\lambda_{1,n} + \lambda_{1,n-1}}{2}\,\frac{R_{1,n} - R_{1,n-1} - a_n(s_n - s_{n-1})}{\Delta x} \qquad (18)$$

if $\lambda_1 > 0$.

To simplify the coding, we define $\lambda_3=u$ and $R_3=s$. The integration step is divided into a predictor and a corrector level. At the predictor level, we go through four steps. Each step is executed at all computational nodes:

1) Computing R_1 and R_2 from (8), λ_1 and λ_2 from (6), and letting $\lambda_3 = u$; computing the stepsize according to the CFL condition.

2) Computing R_{ix} (i=1,2,3) and storing them in such a way that $R_{ix,n}=(R_{i,n+1}-R_{i,n})/\Delta x$.

3) Defining

$$j=n - \frac{1}{2}\,[\mathrm{sgn}(\lambda_{i,n}) + 1] \tag{19}$$

to determine the domain of dependence of R_i and using (14), (15) and (17) after replacing n with j, and (16) as is; denoting any f_i so obtained by f_i^D, and storing them in a double array,

$$f^k_{i,n} = \frac{1}{2}\, f^D_i \tag{20}$$

4) Using $f^k_{i,n}$ to evaluate (13) and then

$$g_n^{k+1/2} = g_n^k + g^k_{t,n}\Delta t \tag{21}$$

for g = a,u,s. Note that (21) performs an update at $\Delta t/2$ only, because of the factor 1/2 in (20).

Boundary conditions, when needed, are enforced between step 3 and step 4. They are discussed in Section 13.

At the corrector level, similar steps are taken. One proceeds without changes till (20), but (20) itself is replaced by

$$f^{k+1/2}_{i,n} = f^D_i - f^k_{i,m} \tag{22}$$

where

$$m=n-\mathrm{sgn}(\lambda_{i,n}) \tag{23}$$

and (21) remains formally the same in the coding but in practice will mean

$$g_n^{k+1} = g_n^{k+1/2} + g_{t,n}^{k+1/2}\Delta t$$

A straightforward but tedious analysis shows that the procedure outlined above has second-order accuracy even with non-constant coefficients [12]. Stability, diffusion and dispersion are easily studied in the isentropic case. By addition and subtraction of the two equations (9), we obtain:

$$\begin{aligned} R_{1t} + \lambda_1 R_{1x1} &= 0 \\ R_{2t} + \lambda_2 R_{2x2} &= 0 \end{aligned} \qquad (24)$$

The two unknowns are now uncoupled. The two equations express the well-known fact that R_1 is conveyed along (u-a)-characteristics and R_2 along (u+a)-characteristics. The analysis can be carried through for each one of the equations, separately. If the technique described above is applied to the second equation, say, it appears that the two parameters G and Ω in the growth factor, $G \exp(i\Omega)$, considered as functions of the wave number, α, behave as shown in Figs. 1 and 2. Waves whose length is larger than four mesh intervals ($\alpha<0.25$) are practically neither diffused nor dispersed. Even waves whose length is comparable to two mesh intervals are little diffused, and almost not dispersed at all, when the Courant number is close to 1 or 2. This is an important feature of the scheme, of which we will take advantage when constructing our computational technique.

A basic FORTRAN code for the scheme described above is presented in Fig. 3.

6. The role of discontinuities

Three types of discontinuities must be considered, in order of increasing severity:

1) Gradient discontinuities, across which all physical parameters are continuous but the derivatives of u, a and p jump.

2) Contact discontinuities, across which s and a jump, but p and u are continuous.

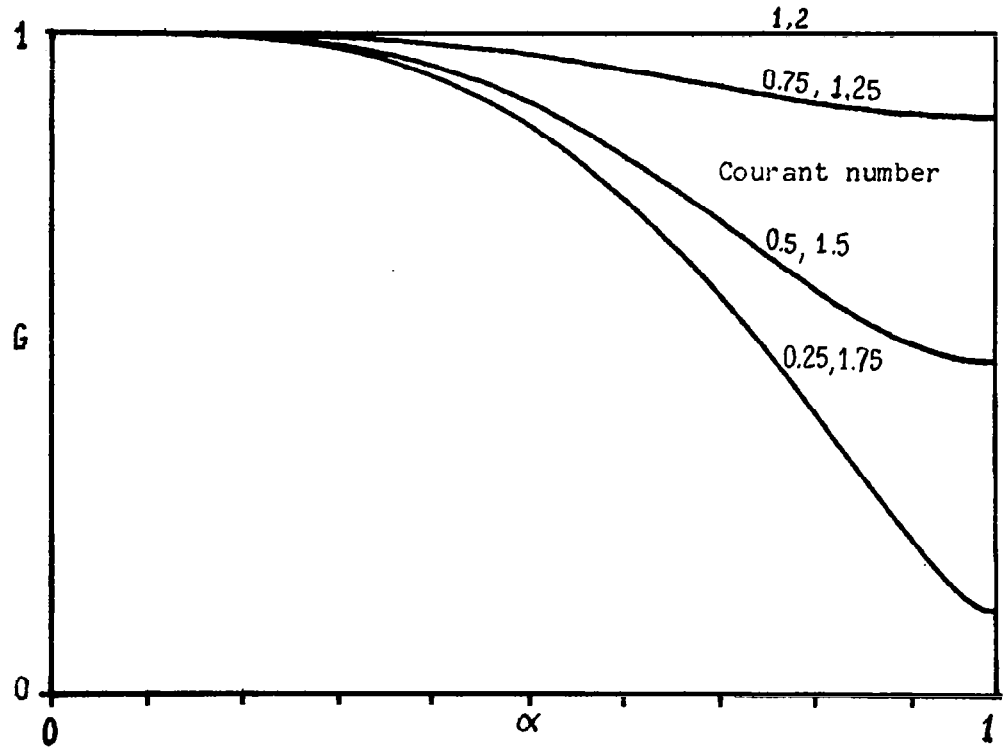

Fig. 1 - Growth parameter for the numerical scheme.

and

3) Shocks, across which u, a, s and p jump.

All discontinuities may be generated at the initial time or along boundaries. Typically, gradient discontinuities are the head and tail of expansion waves which are produced by a discontinuity in the acceleration or the velocity of a piston, or by the sudden removal of a diaphragm. Contact discontinuities are also typically generated at the sudden removal of a diaphragm. Shocks are generated at the initial line as compression waves of finite strength produced by a discontinuity in the velocity of a piston or by the sudden removal of a diaphragm. In addition, contact discontinuities are also generated at the collision of two shocks of opposite families, or when a shock overtakes another shock of the same family, and shocks are also generated within the flow field as a consequence of coalescence of compression waves. Finally, gradient discontinuities are generated at the intersection of shocks or of shocks and contact discontinuities, but in these cases they are sufficiently weak to be neglected.

Discontinuities are generated and supported by the fact that certain signals cannot propagate across them. A computa-

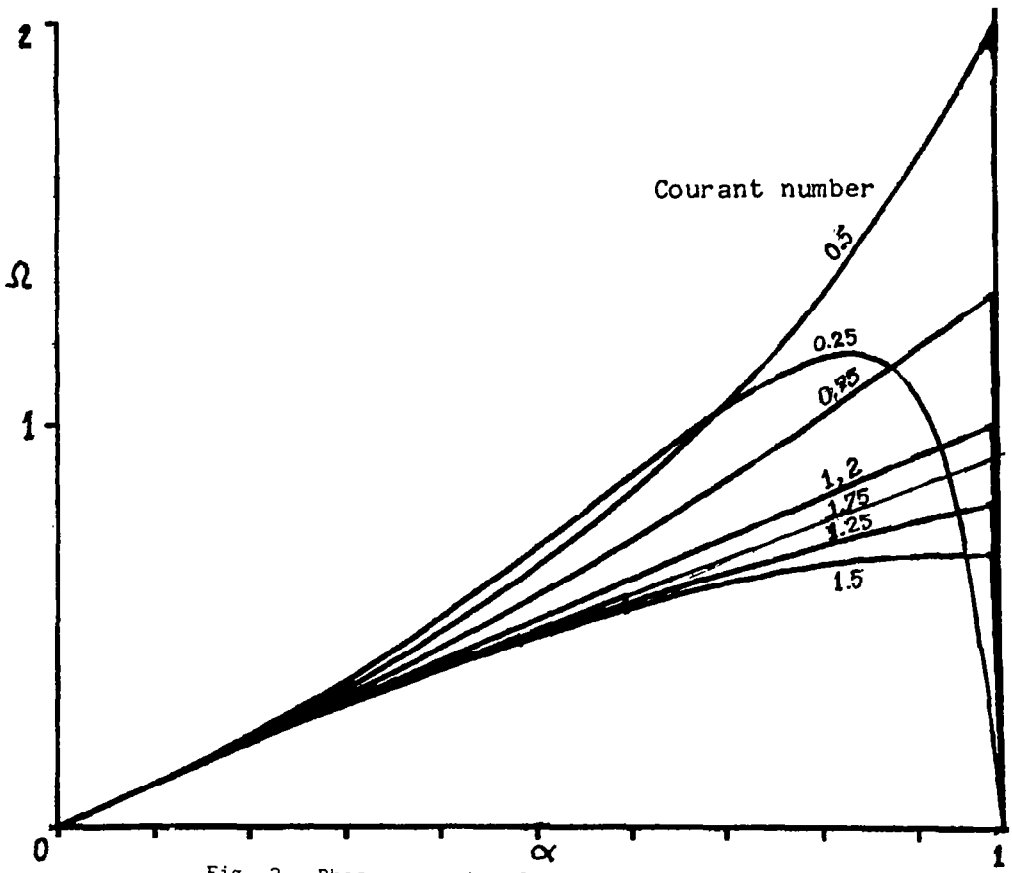

Fig. 2 - Phase parameter for the numerical scheme.

tional code which satisfies the same conditions will automatically make the discontinuities evident. Otherwise, the discontinuities will be spread over several mesh points. With an integration scheme of second-order accuracy, oscillations will appear on either side of the discontinuities, unless special provisions are taken to force monotonicity.

From a mathematical viewpoint, a function of a real variable, continuous with its first derivative (and, if necessary, suitably continued over the entire real axis, periodically or not) can be considered as the real part of a function, analytic on the complex plane (with suitable singularities not lying on the real axis). When such functions are smooth (as the physical parameters, solutions of Euler's equations, are, when discontinuities are removed), their Fourier spectra are dominated by very low frequencies. Therefore, if integration schemes of the type described in Section 5 are used in such a way that they apply only to functions which are continuous with their first derivatives, neither diffusion nor dispersion will occur, and the

```
      DT=CFL
      CFL=10.
      LOOP=-1
   13 DO 1 N=1,NC
      DUM=A(N)*GG
      R(1,N)=DUM-U(N)
      R(2,N)=DUM+U(N)
      AL(1,N)=U(N)-A(N)
      AL(2,N)=U(N)+A(N)
      AL(3,N)=U(N)
      CFL=AMIN1(CFL,STAB*DX/
     1(ABS(U(N))+A(N)))
    1 CONTINUE
      DO 2 N=1,NA
      DO 2 L=1,3
    2 RX(L,N)=(R(L,N+1)-R(L,N))*DDX
      DO 3 N=1,NC
      DO 4 L=1,3
      DUM=1.
      IF(L.EQ.3) DUM=0.
      J=N-(I(L,N)+1)/2
    4 FD(L)=-.5*(AL(L,J)+AL(L,J+1))*
     1(RX(L,J)-DUM*A(N)*RX(3,J))
      FD(4)=-A(N)*U(N)*BPRB(N)
      IF(LOOP.EQ.1) GO TO 5
      DO 6 L=1,4
    6 F(L,N)=.5*FD(L)
      GO TO 3
    5 DO 8 L=1,3
      J=N-I(L,N)
    8 FN(L,N)=FD(L)-F(L,J)
      FN(4,N)=FD(4)-F(4,N)
    3 CONTINUE
      IF(LOOP.EQ.-1) GO TO 10
      DO 11 N=1,NC
      DO 11 L=1,4
   11 F(L,N)=FN(L,N)
   10 CALL BOUND
      DO 12 N=1,NC
      AT=.5*GD*(F(1,N)+F(2,N)+2.*
     1(A(N)*F(3,N)+F(4,N)))
      UT=.5*(F(2,N)-F(1,N))
      ST=F(3,N)
      A(N)=A(N)+AT*DT
      U(N)=U(N)+UT*DT
   12 R(3,N)=R(3,N)+ST*DT
      TIME=TIME+.5*DT
      IF(LOOP.EQ.1) RETURN
      LOOP=1
      GO TO 13
```

Nomenclature

GD	δ	GG	$1/\delta$
CFL	Δt	DT	Δt
STAB	Courant number	R(3,N)	s
BPRB	A_x/A	N	n
NA	number of intervals	NC	NA+1
AL	λ	I(L,N)	$\mathrm{sgn}(\lambda_{i,n})$

Fig. 3 - Basic FORTRAN code for the λ-scheme.

solution will maintain its accuracy and smoothness.

This philosophy, which the senior author has applied in some early papers [13,14,15] is now used again to produce a code which aims to be, at the same time, simple, general and robust. The same philosophy and code can be extended to multi-dimensional problems, whereas codes inspired by [15] are essentially one-dimensional. We will show that all that is required to neutralize the effects of discontinuities and to capture them on a single mesh interval are some elementary switches in the λ-scheme code presented above.

7. Gradient discontinuities

Gradient discontinuities are the weakest type of discontinuities in a flow and, usually, are not considered worthy of a special treatment. It is known that gradient discontinuities travel along characteristics. If u_x and a_x are arbitrarily forced to be discontinuous at (x_o,t_o), R_{1x} and R_{2x} are discontinuous at (x_o,t_o) but, for $t>t_o$, the discontinuity in R_{1x} travels along the (u-a)-characteristic issuing from (x_o,t_o) and the discontinuity in R_{2x} travels along the (u+a)-characteristic issuing from the same point. Therefore, in general, across a gradient discontinuity one of the two Riemann variables is always continuous and differentiable. Its derivative can be approximated using a difference between two points on opposite sides of the discontinuity. The same cannot be said of the other Riemann variable. Therefore, indiscriminate application of the λ-scheme, as exposed in Section 5, in the presence of a gradient discontinuity, can produce inaccuracies. Unfortunately, some of these inaccuracies can pass undetected, unless one disposes of an exact solution for comparison, because they may not affect the local monotonicity of the results. It should be kept in mind that, whereas mesh-dependent oscillations are a sure index of inaccuracy, monotonicity is not necessarily synonymous with accuracy.

A gradient discontinuity with an abrupt change in the slope of R_1, but not of R_2 occurs when $u<a$. If the discontinuity falls somewhere between points A and B, as in Fig. 4a, all x-derivatives of R_1 and R_2 can be approximated correctly, according

to the λ-scheme, except R_{1x} at A. If the discontinuity, however, is exactly at A (Fig. 4b), all x-derivatives can be approximated correctly. Gradient discontinuities generally move and cross over from one interval to another. The calculation benefits from the motion, for two reasons: (i) Often the discontinuity is close to the position shown in Fig. 4b, and the approximation is almost correct; (ii) Also, the error produced at A when the discontinuity is in the position of Fig. 4a is corrected as soon as A is crossed over and starts playing the role of B.

None of the errors produced by the unconditional use of the λ-scheme at a gradient discontinuity seems to be catastrophic. Indeed, if the discontinuity is the front of an expansion wave, the error tends to be diluted, and if it is the front of a compression wave, it soon will give rise to a shock wave, which has to be treated in a different way.

Nevertheless, a few disturbing cases of inaccuracies can occur which justify a mild intervention on the logic of the λ-scheme in the vicinity of a gradient discontinuity, as follows:

1) In the case of Fig. 4a, point A is subject to a perturbation coming from the interior of the advancing wave before the wave front reaches A. In turn (and, again, particularly if the wave front remains for a while to the right of A), the error at A propagates to the point to the left of it, and the perturbation moves at a speed larger than the physical speed of the wave front.

2) The formation of a "precursor" wave in front of the physical wave can also be related to dispersion in the numerical scheme. As shown above, the λ-scheme is non-dispersive for any Courant number between 0 and 2 and low wave frequencies. If a function has a gradient discontinuity, however, its Fourier spectrum is of the order of α^{-2} for increasing α. High order harmonics have a certain relevance (even as not as strong as in the case of jumps, where the spectrum depends on terms of order α^{-1}), and we may expect some dispersion to appear.

3) Stronger effects are expected when the original discontinuity is stronger; that is, particularly when the perturbation

begins as a centered expansion wave.

The discussion will be resumed in Section 24, where examples of unpleasant effects of gradient discontinuities will be given. In the present code, we will modify the λ-scheme to avoid formation of unphysical precursors. To that effect, the derivatives of the Riemann variable which has the gradient discontinuity will be computed from outside the waves at the points immediately outside; the calculation at points inside will not be modified. A local loss in accuracy is inevitable at the points immediately outside the waves, but it does not affect the computation at other nodes. A similar loss in accuracy is necessary to provide

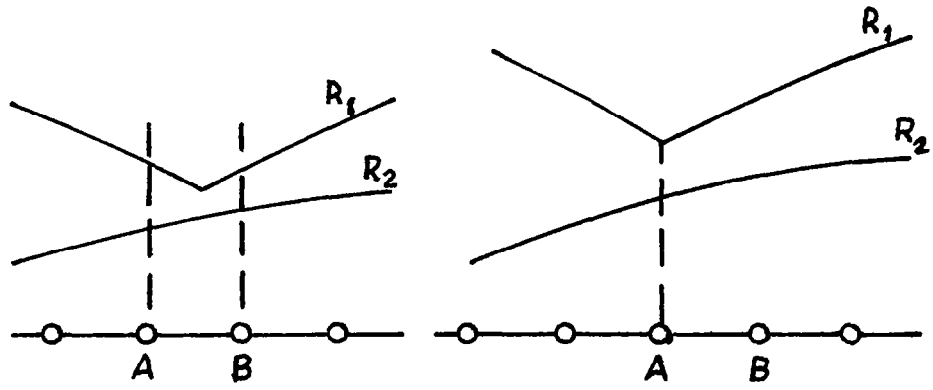

(a) Discontinuity between nodes (b) Discontinuity at a node

Fig. 4 - Behavior of R_1 and R_2 at a gradient discontinuity.

monotonicity in flux difference splitting schemes.

8. Contact discontinuities

In Fig. 5, points A and B again bracket the discontinuity. Now the velocity u and the pressure p are continuous between A and B. Since the entropy is not continuous, it follows that the speed of sound a is not continuous either. A simple relation exists, however, between the speeds of sound on either side of the

contact discontinuity. In the spirit of a discretized code, we assume that the same relation exists between the speeds of sound at A and B (in other words, we assume that the two points are sufficiently close for the pressure to be practically the same at both points):

$$a_A/a_B = \exp[\delta(s_A - s_B)] \tag{25}$$

In trying to determine a_t and u_t at A and B, using (13), we see that, at A, the (u-a)-wave is always proceeding from the discontinuity towards its own left, whereas, at b, the (u+a)-wave is always proceeding from the discontinuity towards its own right. Therefore, f_1 is not directly determinable at A and f_2 is not directly determinable at B. From (25), however, we have:

$$a_{tA}/a_A - a_{tB}/a_B = \delta(s_{tA} - s_{tB}) = \delta(f_{3A} - f_{3B}) \tag{26}$$

Using the first two equations (13) and (26), and letting $u_A = u_B$, f_{1A} and f_{2B} are easily obtained in the form:

$$\begin{aligned} f_{1A} &= \frac{(1-r)f_{2A} + 2f_{1B}}{1+r} \\ f_{2B} &= f_{2A} + f_{1B} - f_{1A} \end{aligned} \tag{27}$$

where

$$r = a_B/a_A$$

Note that the above considerations are correct when both A and B are exactly on the contact discontinuity, on opposite sides of it, regardless of the flow being subsonic or supersonic. In practice, we will force <u>all</u> derivatives at A to be taken from the left and all derivatives at B to be taken from the right. Consequently, f_2 will always be computed correctly at A and f_1 will be computed correctly at B, if the flow at B is subsonic. We must allow for some slight inaccuracy in f_{1B} in supersonic flow; alternatively, we may assume that f_{1B} vanishes identically in supersonic flow.

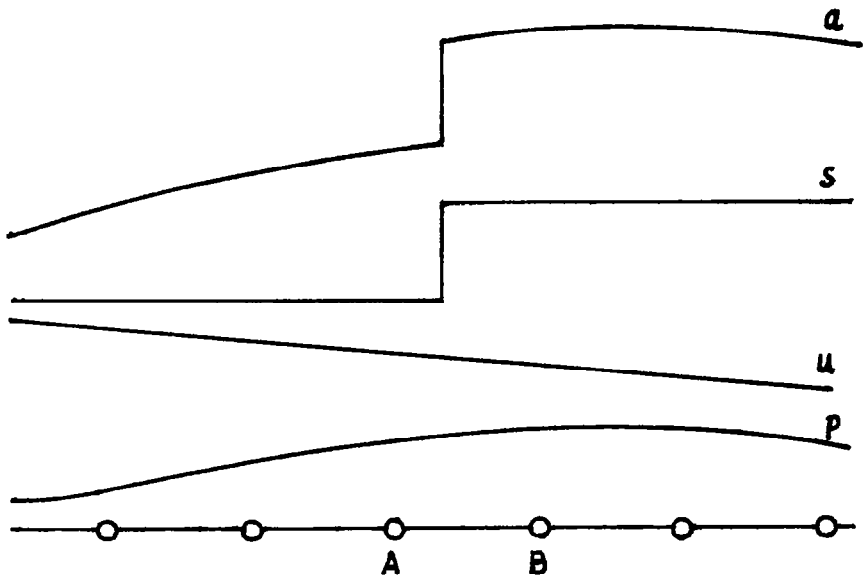

Fig. 5 - Behavior of a,s,u,p at a contact discontinuity.

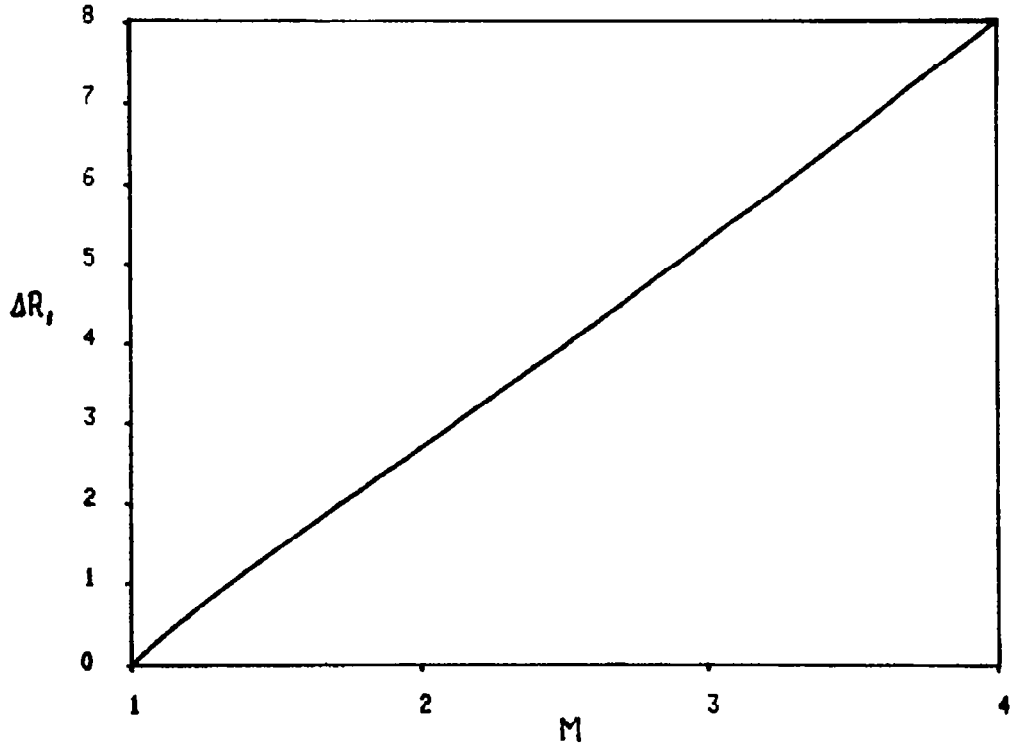

Fig. 6 - Behavior of ΔR_1 as a function of M at a shock.

9. Shocks

The strongest discontinuities occur at shocks. Certain quantities, however, are conserved across a shock. If the shock velocity is denoted by W, then $\rho(u-W)$, $p+\rho(u-W)^2$ and $(u-W)[\gamma p/(\gamma-1)+\rho(u-W)^2/2]$ are the same on both sides of the shock. Such properties of conservation (which are one of the many forms of the Rankine-Hugoniot conditions) may be useful, once the shock velocity, W is known. In an unsteady motion, however, ρu, $p+\rho u^2$ and $u[\gamma p/(\gamma-1)+\rho u^2/2]$ are not continuous across a shock. Differentiating them in space across a shock generates high frequency waves which can be damped only through the use of artificial viscosity, with a consequent loss of accuracy. Other devices proposed to improve accuracy, such as the use of adaptive meshes, have the intrinsic difficulties of shock fitting and it is difficult to extend them to multi-dimensional problems.

The variables used in the λ-scheme are a more natural choice for the analysis of a flow which is about to produce a shock. To make the point, let us obtain analytical expressions for ΔR_1 and ΔR_2 across a shock. Here again, we denote by A and B the points to the left and to the right of the shock, respectively, and assume that $u>0$ and A lies to the left of the shock, so that the high-pressure region (to which B belongs) is to the right of it. Let

$$M = \left(\frac{u-W}{a}\right)_A \tag{28}$$

be the relative Mach number of the shock. Then,

$$\Delta u = a_A \frac{1-M^2}{(1+\delta)M}\,, \quad \Delta a = a_A\left[\frac{(\gamma M^2-\delta)^{1/2}(1+\delta M^2)^{1/2}}{(1+\delta)M} - 1\right] \tag{29}$$

A simple analysis of (29) for values of M close to 1 shows that ΔR_2 is practically continuous across the shock, whereas ΔR_1 tends to grow much faster with M (the behavior of ΔR_1 and ΔR_2 as functions of M is illustrated in Figs. 6 and 7). Therefore, the λ-scheme technique can be used, without having to resort to any special provision, until the shock has formed and has taken up

some strength. The calculation of R_2 at A is correct, not being affected by the presence of the shock; it is also acceptable at B because of the continuity of R_2 across the shock. The calculation of R_1 at both A and B is correct, because R_1 is computed from the left at A (where the flow is supersonic) and from the

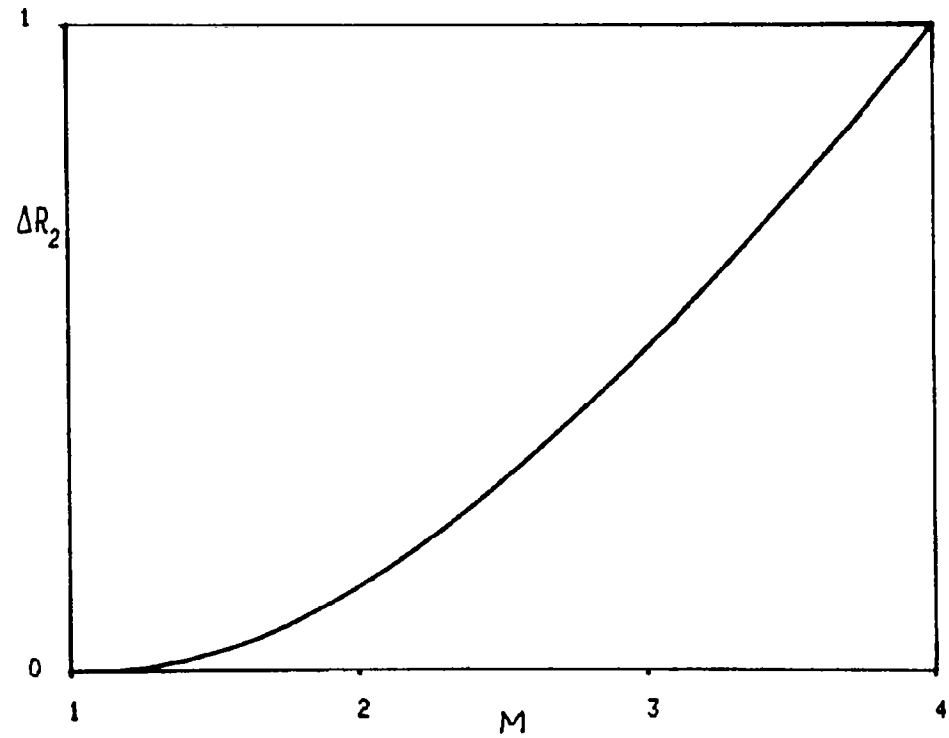

Fig. 7 - Behavior of $\Delta R_2'$ as a function of M at a shock.

right at B (where the flow is subsonic).

When the shock is about to form, we have indeed all the elements which are necessary to detect its formation, and all of them are accurate. For the detection of the shock, it is convenient to compute the parameter:

$$\Sigma = \frac{R_{1B}-R_{1A}}{a_A} \tag{30}$$

Between M=1 and M=4, Σ is a linear function of M to within 1%. The exact relation between Σ and M, obtainable using (29), is

$$\Sigma = \frac{[(\gamma M^2-\delta)(1+\delta M^2)]^{1/2} + \delta(M^2 - 1)}{\delta(1+\delta)M} - \frac{1}{\delta} \qquad (31)$$

which can be approximated, for $1 \leq M \leq 4$, by the linear function:

$$M = 1 + g\,\Sigma \qquad (32)$$

where g is defined by computing (32) at M=4:

$$g = \frac{4\delta(1 + \delta)}{11\delta-4+[(16\gamma-\delta)(1+16\delta)]^{1/2}} \qquad (33)$$

The detection of the shock is performed by computing Σ at every point, as defined by (30), and then by applying (32) to obtain an approximate value of M. If M is less than 1.1, say, the interval is considered as shockless; otherwise, the interval will be labelled as carrying a shock, as it will be explained below.

When a shock is known to exist, it is computed in a similar way, as follows. A first estimate of M is made, using (30) and (32). Then a new value, Σ_1 of Σ is obtained from

$$\Sigma_1 = 2\,\Sigma - \Sigma'$$

where Σ' is computed from (31), using the first approximation for M. Finally, (32) is applied once more, using Σ_1, and the evaluation of M is now accurate to within 10^{-3}. If more accuracy were needed, the procedure can be repeated once more. To support our conclusions, errors produced by using (32) alone, and by applying one or two iterations are plotted in Fig. 8 and labelled E_1, E_2 and E_3, respectively. For a given M, the error is the difference between the given Σ and Σ obtained from (31).

Once the shock Mach number has been obtained, the shock velocity, W, follows from (28), and the values at B can be updated using the Rankine-Hugoniot conditions, expressed by (29) and by

$$s_B = s_A + [\ \ln \frac{\gamma M^2-\delta}{1+\delta} + \gamma\ \ln \frac{1+\delta M^2}{(1+\delta)M^2}]/(2\gamma\delta) \qquad (34)$$

It must be noted that correct values of f_2 and f_3 are needed at B, to be used in the corrector stage for the calculation of the point to the right of B. Such values can be obtained by computing u_t and s_t numerically, and using the second and third of (13).

Finally, it is very important to note that the calculation of the relative Mach number, as outlined above, does not change if the high pressure side of the shock lies to the left of the discontinuity, provided that R_2 and R_1 are interchanged and the indices A and B are interchanged as well. This is because the change in sign in u in the definition of Σ is compensated by a change in sign in M.

A basic FORTRAN code for the calculation of the shock is presented in Fig. 9.

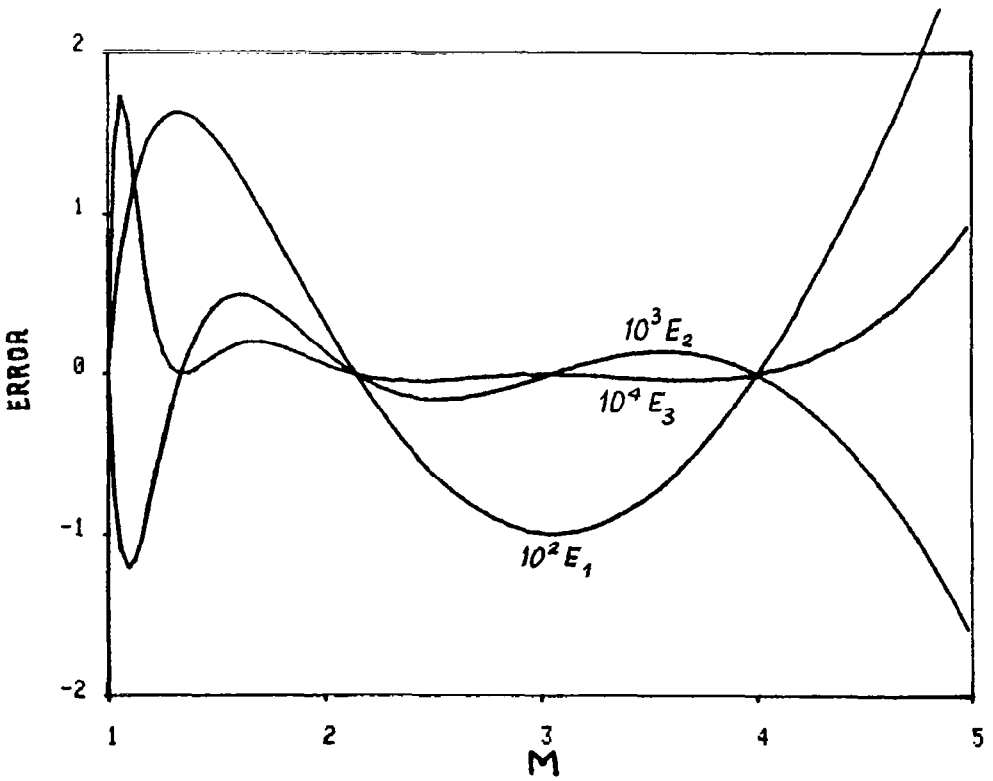

Fig. 8 - Errors in successive approximations of $\Sigma(M)$ using equation (32).

```
      L1=3-L
      LL=L-L1

      NN=N+L-1
      NM=NN-LL
      SIGMA=(R(L,NN)-R(L,NM))/A(NM)
      TM=1.+G1*SIGMA
      SM=TM**2
      SIGMA=2.*SIGMA-SQRT((GAMMA*SM-GD)*(1.+GD*SM))+
     1GD*(SM-1.))/(GE*TM*GD)+GG
      TM=1.+G1*SIGMA
      SM=TM**2
      SN=R(3,NM)+(ALOG((GAMMA*SM-GD)/GE-GAMMA*ALOG(GE*SM/
     1(1.+GD*SM)))/(2.*GD*GAMMA)
      XBT(J)=U(NM)-A(NM)*TM*LL
      R1(L1,NN)=R(L,NN)-2.*(A(NM)*(SM-1.)/(GE*TM)-LL*U(NM))
      UN=.5*(R(2,NN)-R(1,NN))
      F(L1,NN)=LL*2.*(UN-U(NN))/DT+FL(L,NN)
      F(3,NN)=SN-R(3,NN))/DT
      RETURN
```

Nomenclature

GD	δ	GG	$1/\delta$
GE	$1+\delta$	G1	g defined by (33)
SIGMA	Σ	DT	Δt
TM	M	R(3,N)	s
GAMMA	γ	XBT	x_t*

Fig. 9 - Basic FORTRAN code for shock calculation.

10. Shocks in the presence of a contact discontinuity

The calculation of a shock must be modified when a contact discontinuity belongs to the same interval as the shock. In Fig. 10, a possible configuration of this type is shown by a plot of the entropy distribution. In the same interval, AB, a contact discontinuity (C.D.) and a shock coexist. If the technique described in Section 9 were applied without modifications, the entropy jump across the shock would be automatically assumed as the one between A and B, instead of the real one, denoted by (S).

Let

$$\Sigma_o = \frac{R_{1A} - R_{1B}}{a_B} \tag{35}$$

as it would be evaluated in Section 9, using (30). The proper value of Σ should be, instead,

$$\Sigma = \frac{R_{1S} - R_{1A}}{a_A} \tag{36}$$

Let

$$\Delta = e^{\delta(S_S - S_B)} \tag{37}$$

Then,

$$\Sigma = \Sigma_o + \frac{a_B}{\delta a_A}(\Delta - 1) \tag{38}$$

since the pressure is constant across the contact discontinuity.

A trial-and-error routine can be used, in which a first guess is made of S_S, Δ is obtained from (37), Σ from (38), M from

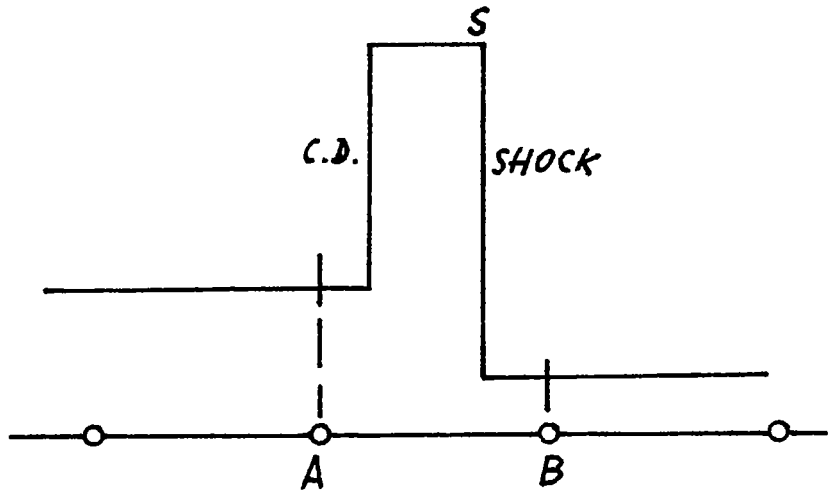

Fig. 10 - Shock and contact discontinuity in the same interval.

(32), and an error results by comparing the guessed S_S with S, as obtained from the right-hand side of (34).

11. Sonic interval

Let $u > 0$ and the flow be subsonic at a point, A and supersonic at the next point, B (Fig. 11). No discontinuity occurs in the interval, AB. Nevertheless, the computation must be performed with a certain care. Both derivatives of R_1 and R_2 at A and B are computed as prescribed by the λ-scheme. What we cannot do as usual is the averaging of λ_1, as shown in (17), and the correction of f_1, as shown in (22). Indeed, the prescription would carry certain information from A to B and from B to A which should not cross over the sonic point. Consequently, λ_1 and the correction to f_1 are used with their local values at A and B.

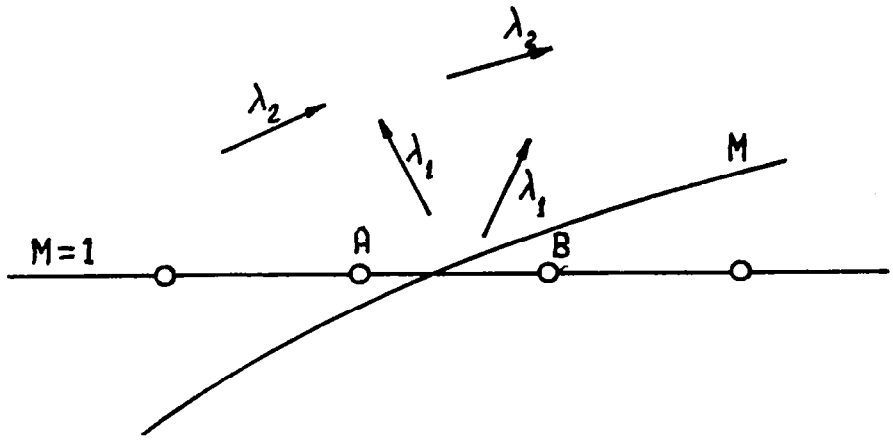

Fig. 11 - Interval containing a sonic point.

12. Tracking discontinuities

We have seen how the basic λ-scheme must be modified locally at one end or both ends of an interval containing a discontinuity and which additional algebra is needed for certain discontinuities. We discuss now a simple and general way of tracking any number of discontinuities.

Every point, x = (n-1) Δx (n≥1), is denoted by an index, IN(N) (in FORTRAN notation), which encodes the nature of the discontinuity or discontinuities, present in the interval to the right of the point. By a simple device, one single index can describe an interval containing more than one discontinuity, without ambiguities. Let the discontinuities be denoted by increasing powers of 2, II(L) = 2**L (in FORTRAN notation again), as follows:

L=1,	II=2,	a shock with the low-pressure region on the left.
L=2,	II=4,	a shock with the high-pressure region on the left.
L=3,	II=8,	a contact discontinuity.

L=4,5 II=16,32, gradient discontinuities carried by right-running characteristics.

L=6,7 II=64,128, gradient discontinuities carried by left-running characteristics.

In addition, we will use the number 256 (corresponding to L=8) to denote an interval in which the flow velocity changes from subsonic to supersonic.

In the binary system used by computers, any power of 2 is represented by a 1, properly located. For example,

2	is represented by	10
4	"	100
8	"	1000
16	"	10000
32	"	100000 , etc.

The coexistence of two or more discontinuities in a single interval will bring in more than one power of 2. For example, if one high-to-low pressure shock,one contact discontinuity and two left-running gradient discontinuities exist in the same interval (as at the sudden removal of a diaphragm), such an interval will be denoted by

IN(N) = 4 + 8 + 64 + 128

that is, by IN(N)=204, but in binary notation this number will be

IN(N) = 11001100

It is clear, thus, that the index still preserves the individuality of all discontinuities. To reveal each one of them, separately, it will be sufficient to perform a logical .AND. between the index, IN(N) and the pertinent II(L). In FORTRAN notation, if

IN(N) . AND . II(L)

is true, the interval contains the discontinuity denoted by 2^L.

To summarize, the new appearance of a discontinuity denoted by II(L) with $1 \leq L \leq 7$, or of a sonic point, denoted by II(8), entails a Boolean sum to be coded in FORTRAN as

IN(N) = IN(N) . OR . II(L)

The disappearance of a discontinuity or of a sonic point will be coded as

IN(N) = IN(N) . AND . (. NOT . II(L))

A discontinuity or a sonic point will be detected by a logical IF:

IF (IN(N) . AND . II(L))

with the expression being true.

All the operations described above are unambiguous and are not time consuming. Note that arithmetic sums cannot be substituted for Boolean sums. For example, the coalescence of a shock (2) and a contact discontinuity (8) would generate a 10, which could also be interpreted as denoting the presence of a shock (2) and two other shocks (4+4).

Note also that two values of L are assigned to either type of gradient discontinuity. Such a redundance is necessary only to distinguish between the head and the tail of an expansion wave, when they belong to the same interval, as it happens when a centered expansion wave is generated. Head and tail move at different speeds; therefore, they must be considered as different discontinuities.

The information concerning discontinuities is stored in two arrays, depending on an index, J. The first array contains the location, x^*, of the discontinuity within the interval ($0 \leq x^* \leq \Delta x$); the second array contains the speed at which the discontinuity moves (x_t^*). Such information is not used in actual updating of physical parameters. It is only applied to detect the crossing of a discontinuity from one interval to a neighboring one. This happens whenever x^* becomes negative or larger than Δx. The position of the discontinuity within the interval is, of course, updated using its velocity.

The velocity of a discontinuity, in turn, is easy to obtain. For a gradient discontinuity, the velocity is u+a or u-a; for a contact discontinuity, it is u; and the shock velocity, W, is computed from (28).

In the arrays, the information is stored considering each interval in order, from N=1 on. As an interval appears which contains discontinuities, the pertinent information is stored in the J-arrays in order of increasing L. Obviously, when neeeded, such information must be retrieved in the same order.

13. Treatment of boundaries

Different problems require different modeling of boundary conditions, but the basic requirements at boundaries (regardless of their nature) are always the same. If we turn back to Eqs. (12), and assume that $u>0$ and the flow is subsonic, we see that at the left boundary f_2 and f_3 should be computed from outside; consequently, they must be considered as unknown. Similarly, at the right boundary f_1 should be computed from outside and, therefore, must be considered as unknown. If the flow were supersonic, f_1, f_2 and f_3 are all unknown at the left boundary and known at the right boundary.

The modeling of the boundaries provides the codes necessary to determine the unknowns without introducing arbitrariness and conserving the same computational accuracy as at interior points.

In the present study, we consider only open (permeable) boundaries, as follows:

1) In strictly one-dimensional problems (flows in ducts of constant cross-sectional area), we assume that both the left and the right boundary are reached only by simple waves. In addition, we stipulate that the flow outside the left boundary is homentropic. Therefore, at the left boundary, $f_3 = 0$ and f_2 is also equal to 0 because R_2 is a constant throughout the left-running simple wave. For a similar reason, $f_1 = 0$ at the right boundary.

2) In ducts of variable cross-section, we consider only nozzles connecting two infinite reservoirs. In the one at the left, the flow is at rest, with a uniformly distributed stagnation temperature and a constant entropy. The second condition obviously provides again $f_3 = 0$. To apply the first, let us recall that, in a steady flow,

$$a_o^2 = a^2 + \delta u^2 \tag{39}$$

The time-derivative of (39) at the entrance of the duct must reflect the fact that a_o is constant outside; thus,

$$a\, a_t + {}^{\delta} u\, u_t = 0 \tag{40}$$

at the first computational node. By comparison of (40) with the first two Eqs. (13), we obtain

$$f_2 = \frac{(u-a)f_1 - 2af_4}{u + a} \tag{41}$$

In the reservoir at right, we assume that the pressure is constant. Such an assumption does not imply that the speed of sound is also constant, since the entropy may vary inside the duct, due to the formation and motion of shocks. We must now combine (10) with the first and the third of (13) to find

$$f_1 = - f_2 - 2f_4 + 2aP_t/\gamma \tag{42}$$

3) If the flow is supersonic at the left boundary, we assume that it is uniform outside; therefore all f_i equal 0.

14. Outline of the computational code

In addition to a main program, which serves as a general organizer, the code contains three sets of subroutines.

Gasdynamical Subroutines

MARCH - provides the basic integration scheme as described in Section 5, with some additional features:

a) reducing the stepsize if a discontinuity is travelling over two mesh intervals.

b) calling TEST to detect sonic points and formation of shocks.

c) calling BOUND to enforce boundary conditions.

d) calling TRACK to treat discontinuities.

e) calling XING to provide for shifting of discontinuities from one interval to the next.

TEST - detects sonic points and the formation of shocks.

TRACK - computes contact discontinuities according to Section 8, calls SHOCK and contains some instructions for the interaction of contact discontinuities and shock and of two wave fronts.

SHOCK - computes shocks according to Sections 9 and 10.
BOUND - computes boundary conditions according to Section 13.

Logical Subroutines

XING - provides the logic for the crossing of discontinuities from one interval to the next; if necessary, it calls the following subroutines:
INSERT - when a new discontinuity appears,
DELETE - when a discontinuity disappears,
SWITCH - which accomodates x^* and x_t^* in their general arrays according to the new position of the discontinuity,
COUNT - which provides the necessary bookkeeping when two discontinuities from two neighboring intervals are interchanged.

Initial Condition Subroutines

XMP, XMQ and XMR - provide different types of initial conditions for the examples shown in Sections 15 through 28 and, when available, the exact solutions to the problems.

Additional Logic

A few additional logical statements are added to the code, which are justified by the following considerations.

If two discontinuities (or more) appear in two consecutive intervals, we distinguish two cases:

1) The discontinuities are the head and the tail of the same expansion wave. In this case the calculation may proceed according to the logic outlined above. The special provisions for the treatment of gradient discontinuities do not conflict with each other.

2) In all other cases, the point bracketed by the discontinuities may receive successive instructions which are inconsistent with each other. Instead of going through the cumbersome analysis of all possible cases, we prefer to skip the calculation of the point. Since all discontinuities move, the point will be restored to normality at the next step. When such a situation arises, we cut the stepsize in half, in order to reduce

the period of neglect.

Across a contact discontinuity, u does not change. Therefore, in principle, the speed of the discontinuity may be taken as the value of u at the point to the left of the discontinuity or to the right of it. We use the second option in all cases except one, that is, when the contact discontinuity is in the same interval as a shock having the high pressure on the left.

When a contact discontinuity crosses from one interval to the next, the entropy at the point which has been crossed over must be changed into the value pertinent to the other side of the discontinuity and the speed of sound has to be recomputed according to (25).

15. Test cases. Strictly one-dimensional flows

To test the efficiency of the logic of the code, we chose the following problems in which the mechanics of the flow is not complicated by variable area effects:

1) Collapse of an expansion shock.
2) Head-on collision of two shocks.
3) Riemann's shock tube problem.
4) Merging of two shocks of the same family.
5) Decaying shock.
6) Interaction of a shock and a contact discontinuity.
7) Interaction of two expansion waves.

Problems 1,2,3 and 4 have also been treated in [9] (cases c,i,f, and i again), and we have tried to use the same data to make the comparison between our results and the results of [9] as easy as possible.

Our demonstrative displays consist essentially of two figures for each case: a comparison of computed values (denoted by O's) and exact values of ρ (solid lines) at a given time, whenever an exact solution is available, and a tracking of discontinuities, as computed, in the (x,t)-plane. Discontinuities are labeled with the same values of L as used in Section 12. Occasionally, we will also present sets of lines of constant den-

sity (isopycnics) in the (x,t)-plane.

16. Collapse of an expansion shock

This test, as mentioned in [9], is meant to check the ability of the computational code to avoid producing unphysical expansion shocks. We start assuming that an expansion shock exists, and let it collapse. Initially, the flow proceeds from a uniform region 1 (defined by a subsonic Mach number, M_1, a speed of sound, $a_1 = [\gamma/(1+\delta M_1^2)]^{1/2}$, and an entropy, $s_1 = 0$), into a uniform region 2, crossing a shock in reverse. The values in region 2 are obtained using the Rankine-Hugoniot conditions across the expansion shock. The correct flow consists of a left-running expansion wave, joining region 1 to a uniform region 4, a contact discontinuity, separating region 4 from a uniform region 3, and a

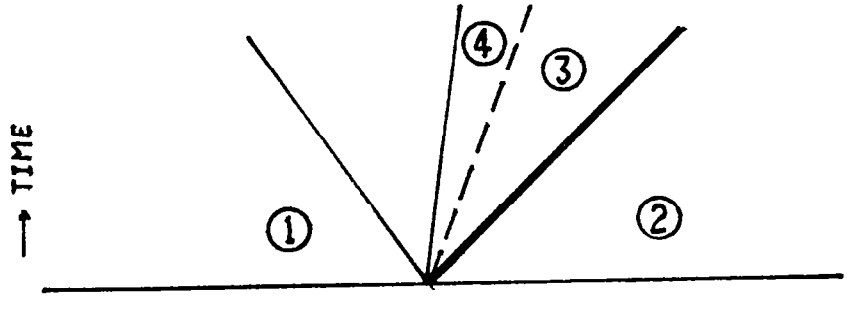

Fig. 12 - Collapse of an expansion shock.

very weak shock, separating region 3 from region 2 (Fig. 12). Across the wave, $a_1+\delta u_1 = a_4+\delta u_4$, and $P_4 = P_1+(\gamma/\delta)\ \ln(a_4/a_1)$. In addition, $u_3=u_4$, $P_3=P_4=P_2+\ln[(\gamma M^2-\delta)/(1+\delta)]$, if M is the Mach number of the weak shock. Finally, W being the shock velocity, $M_2 = (u_2-W)/a_2$ and $(u_3-W)/(u_2-W) = (1+\delta M^2)/[(1+\delta)M^2]$. These equations allow an exact solution to be evaluated by trial-and-error. The case presented here corresponds to $M_1=0.5$. Initially, the index (IN) for the interval containing the expansion shock is set equal to 200 (8+64+128). Fig. 13 shows $\rho(x)$ at t=0.3100, Fig. 14 shows the tracking of the wave fronts (6 and 7), of the sonic point (8) and of the contact discontinuity (3) between t=0 and t=0.3100. Fig. 15 shows the isopycnics for the same interval of time. We note:

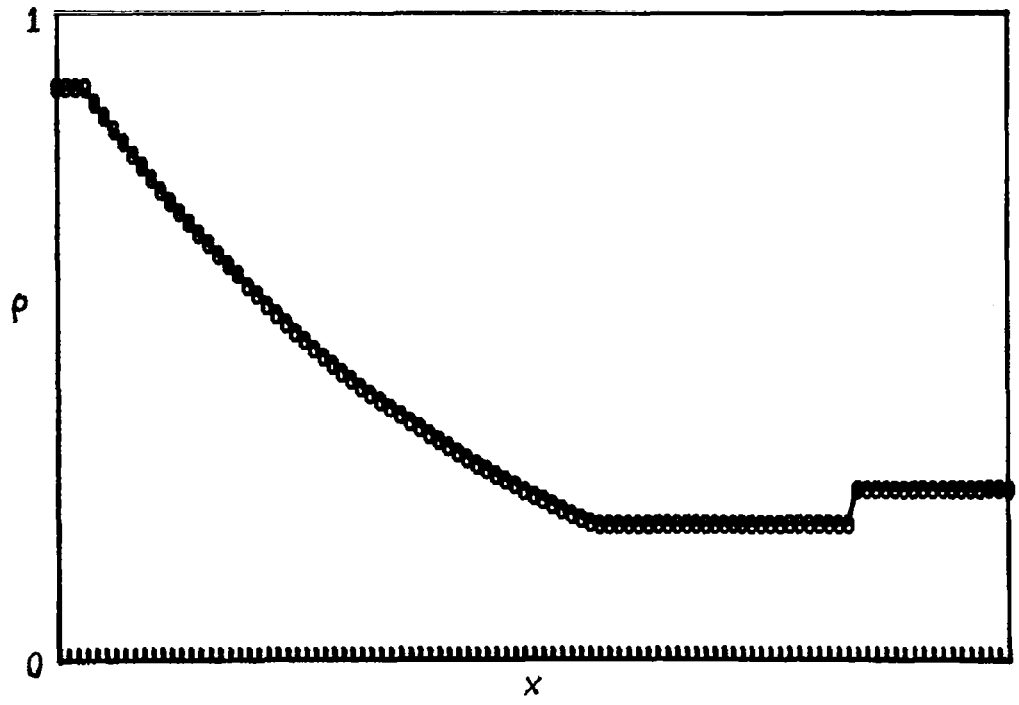

Fig. 13 - Exact and computed density in the collapse of an expansion shock (100 intervals).

1) Perfect adherence of the computed values to the exact values.

2) No overflowing of perturbations across the wave front, either in form of oscillations (as in non-upwind schemes and in the original λ-scheme) or in form of monotonic smearing (as in [9]).

3) No inaccuracies at the sonic point.

4) Perfect capture of the contact discontinuity.

5) The weak shock (which, at t=0.3100, is out of the picture already) is not tracked, for being too weak. Nevertheless, at previous times, a minor jump in ρ reveals it.

In runs 102 and 103, the number of intervals has been changed to 50 and 25 respectively. Some deterioration, particularly near the wave front, is expected and it is evident in Figs. 16 and 17. In Fig. 18, four typical stages in the evolution of the flow are presented, as superimposed plots of $\rho(x)$ for different values of t, in Run 103.

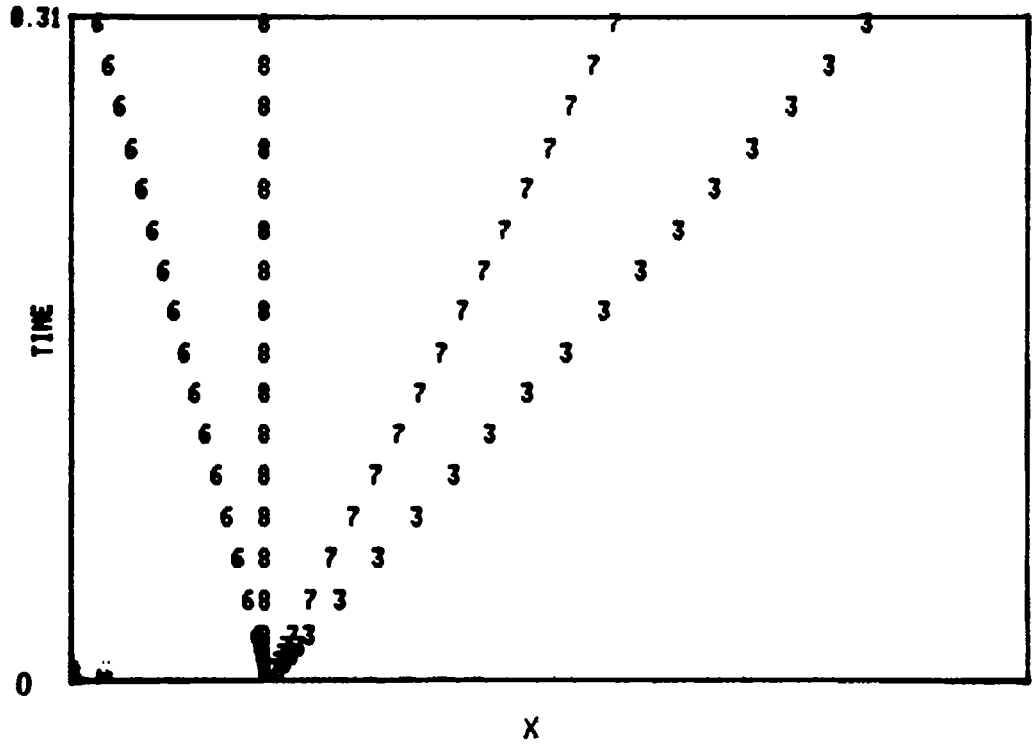

Fig. 14 - Tracking of discontinuities in the collapse of an expansion shock.

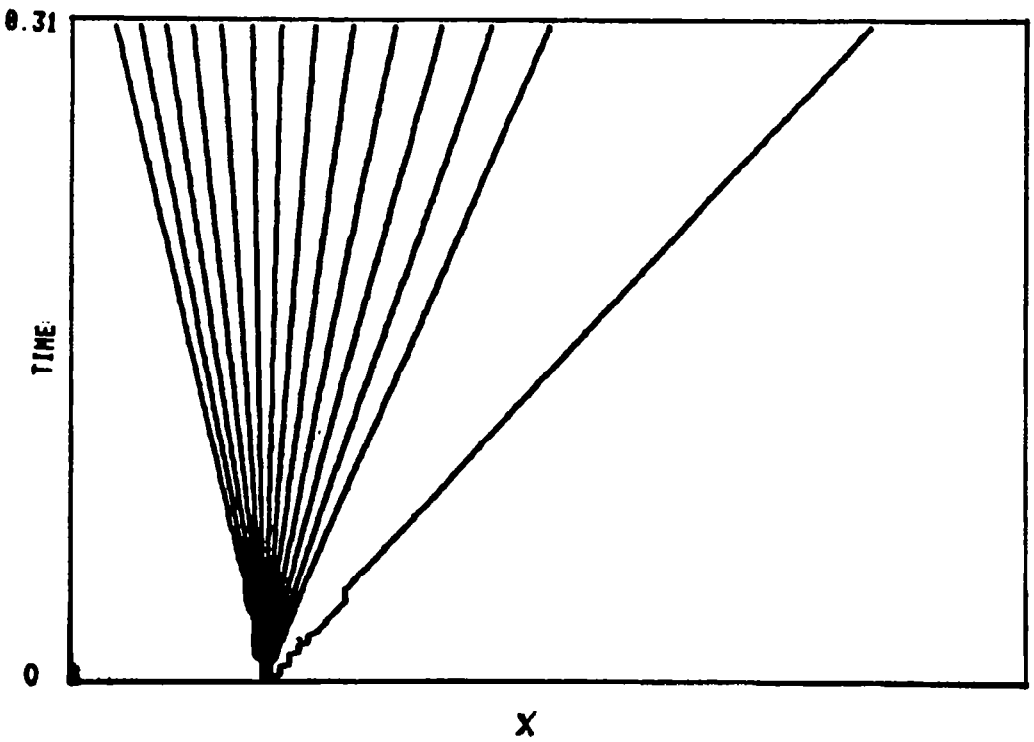

Fig. 15 - Isopycnics in the collapse of an expansion shock.

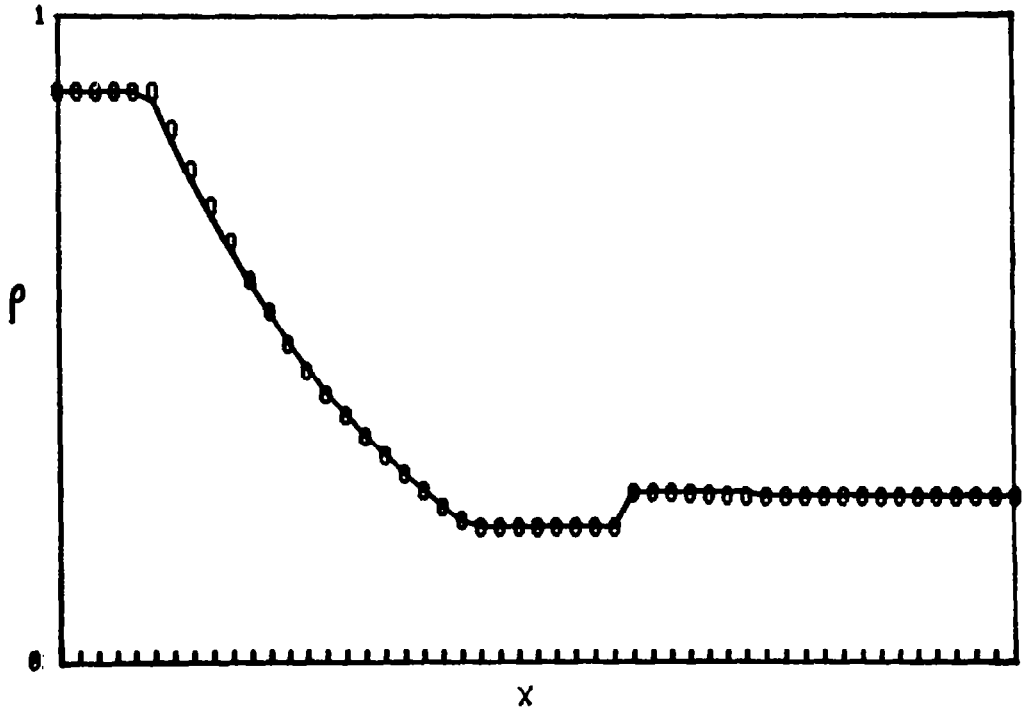

Fig. 16 - Density after the collapse of an expansion shock (50 intervals).

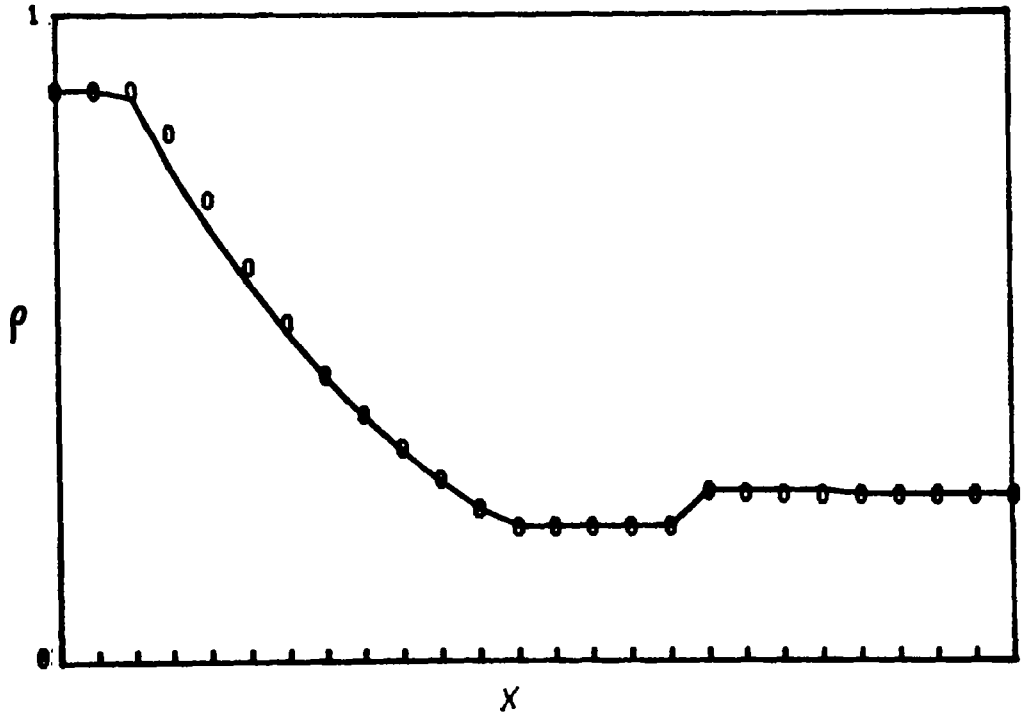

Fig. 17 - Density after the collapse of an expansion shock (25 intervals).

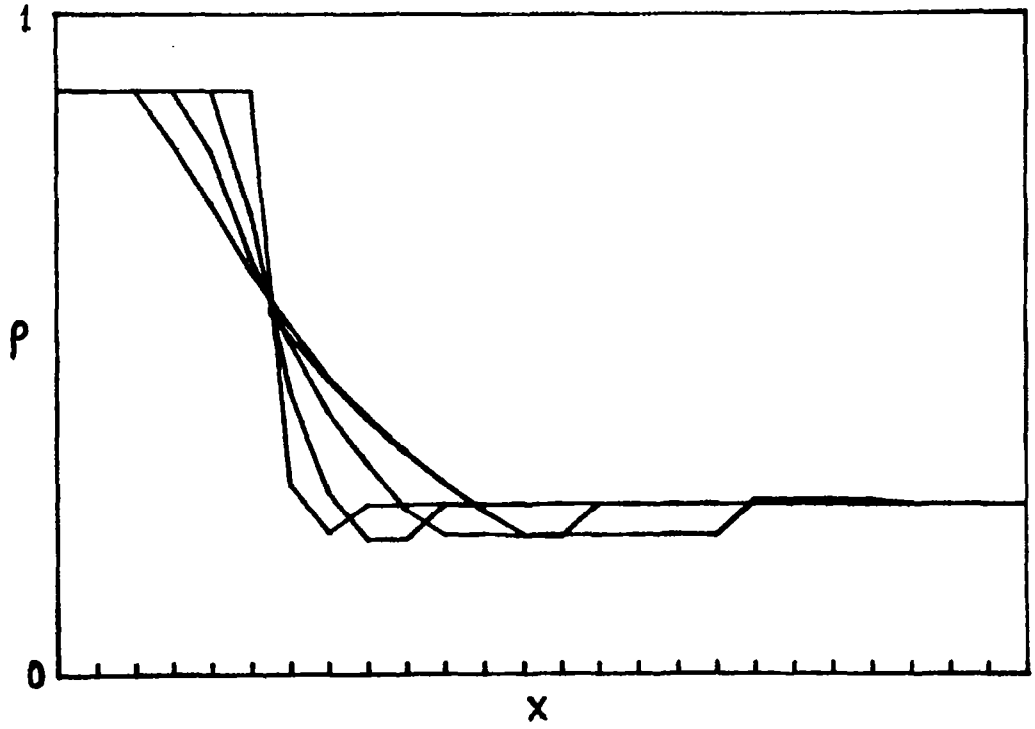

Fig. 18 - Evolution of $\rho(x)$ in time in collapse of an expansion shock.

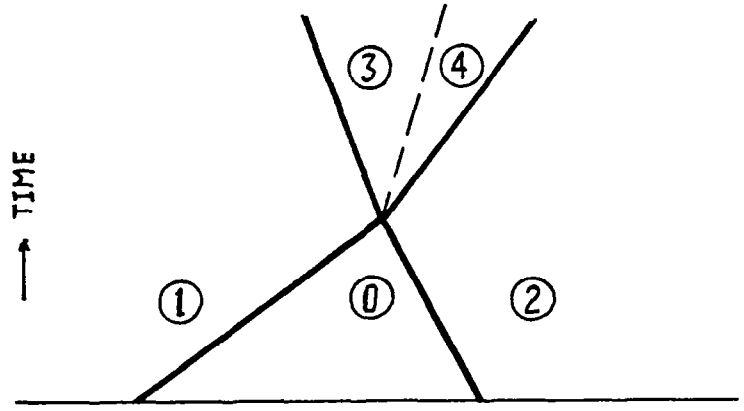

Fig. 19 - Head-on collision of two shocks.

17. Head-on collision of two shocks

Here we start assuming the existence of a right-running shock, separating a high pressure region (1) of uniform flow from a low-pressure region (0) also uniform, and of a left-running shock, separating region 0 from another high pressure region, labeled 2, also uniform. The two shocks will collide and continue moving in their original directions, at different speeds. A contact discontinuity will also appear (Fig. 19). For the exact solution, the new shock velocities and the physical parameters in regions 3 and 4 are obtained by trial-and-error, using the Rankine-Hugoniot conditions on the two new shocks and imposing $P_3=P_4$, $u_3=u_4$. The case presented here (Run 201) corresponds to a right-running shock defined by M=2 and a left-running shock defined by M=1.5. The computation is performed on 50 intervals. Initially, we set IN=2 in the interval containing the right-running shock and IN=4 in the interval containing the left-running shock. Fig. 20 shows $\rho(x)$ at t=0.3107 and Fig. 21 shows the tracking of the two shocks. The contact discontinuity is not tracked for being too weak; it is, however, detectable as a minor step in Fig. 20. Fig. 22 shows some plots of $\rho(x)$ at successive times just before and just after the collision.

18. Riemann's problem

This is a classical case, in which, consequent to an initial jump in pressure, a left-running expansion wave, a contact discontinuity and a shock are generated (Fig. 23). The same relations are satisfied as for the previous case of an expansion shock, and an exact solution can be obtained accordingly. The case presented here corresponds to an initial pressure ratio equal to 10 and uniform temperature throughout (so that the entropy is lower in region 1 than in region 2). Initially, the interval where the pressure jumps occur has IN=202. In this case (Run 301), 100 intervals were used. Fig. 24 shows $\rho(x)$ at t=0.0128, Fig. 25 shows the discontinuities, and Fig. 26 the isopycnics. The computed shock, in Fig. 24, appears slightly ahead

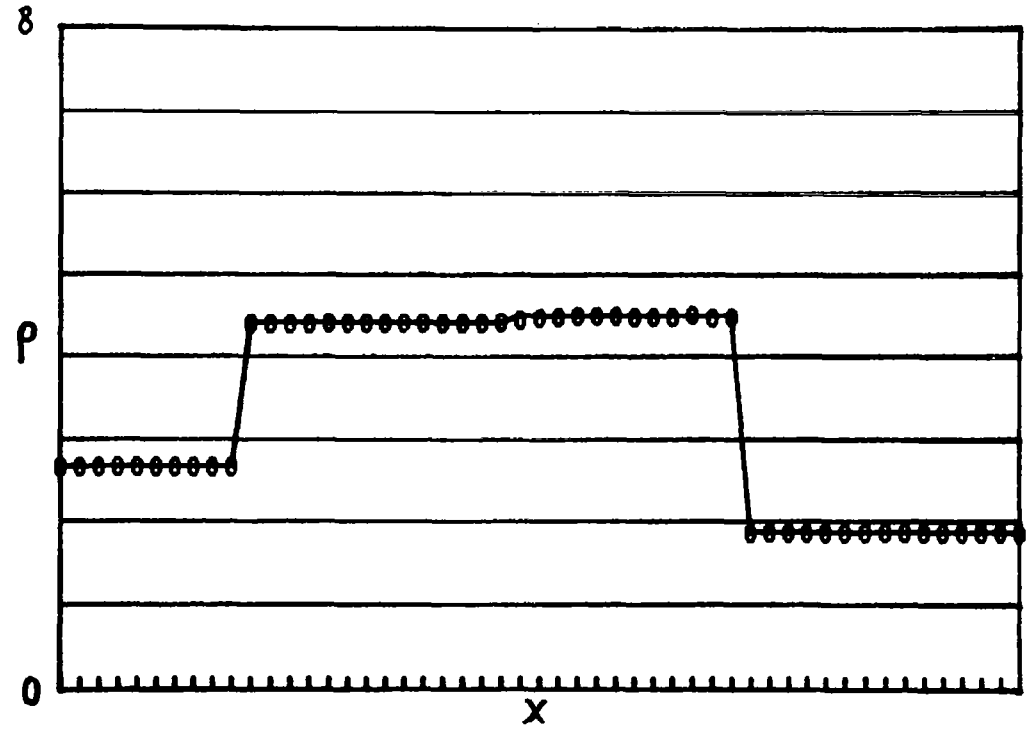

Fig. 20 - Density after the head-on collision of two shocks.

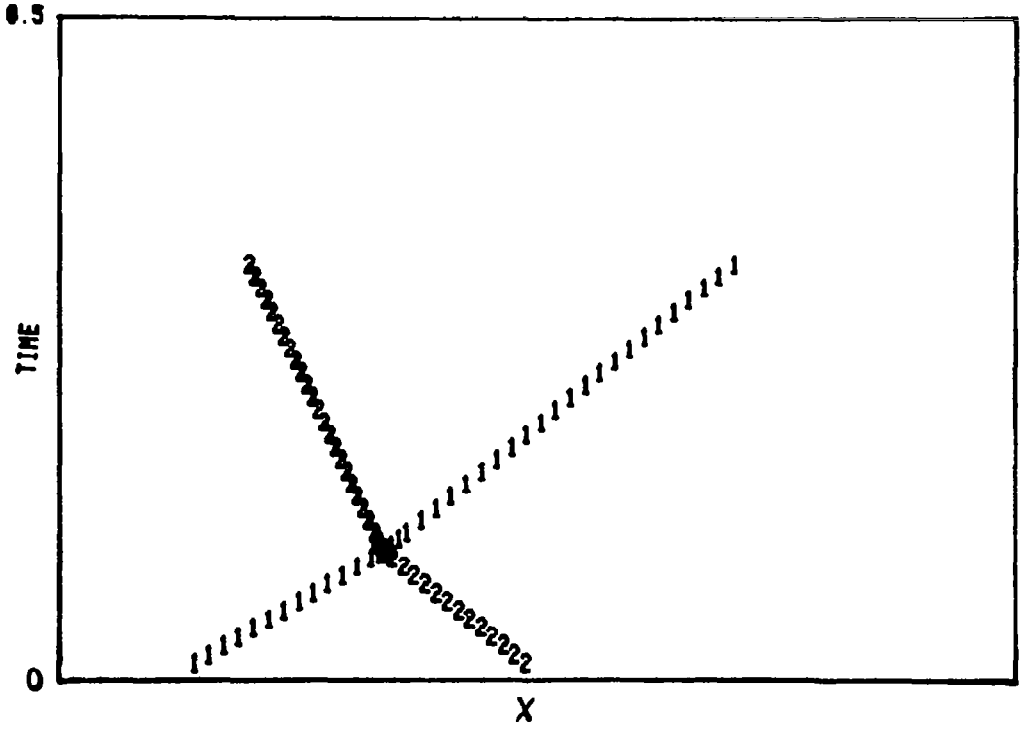

Fig. 21 - Tracking of shocks in head-on collision.

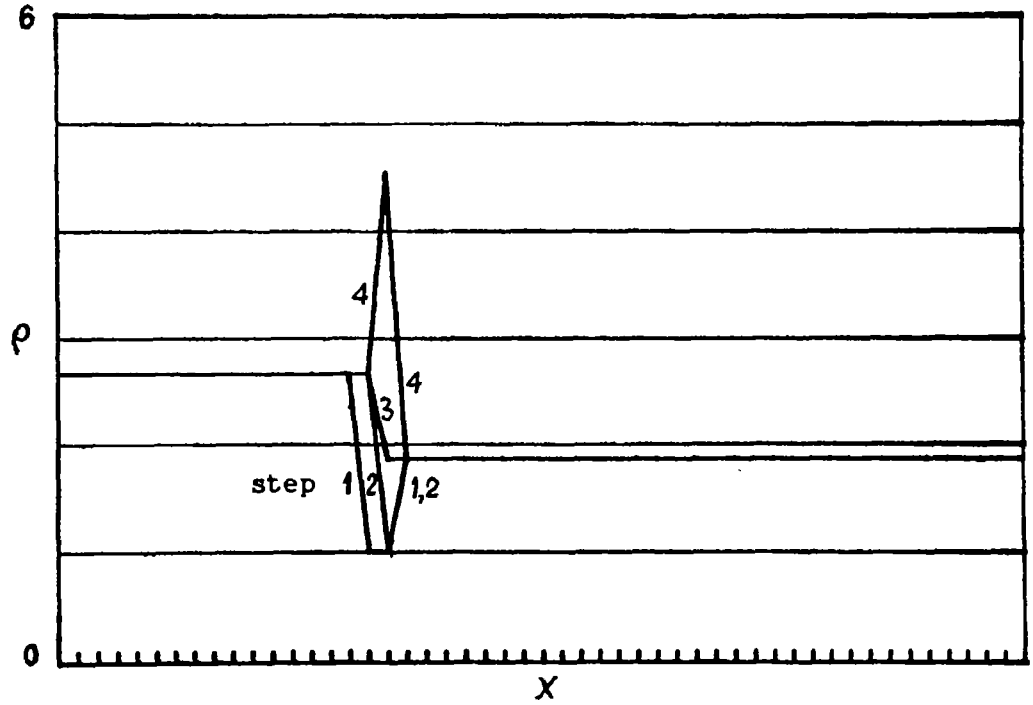

Fig. 22 - Evolution of $\rho(x)$ in the collision of two shocks.

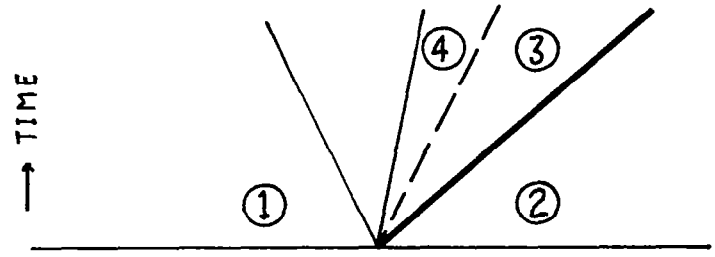

Fig. 23 - Riemann's problem.

of the exact shock. This is due to an initial uncertainty in the location of the shock within the interval and it may or may not appear in plots, according to the location of the exact shock

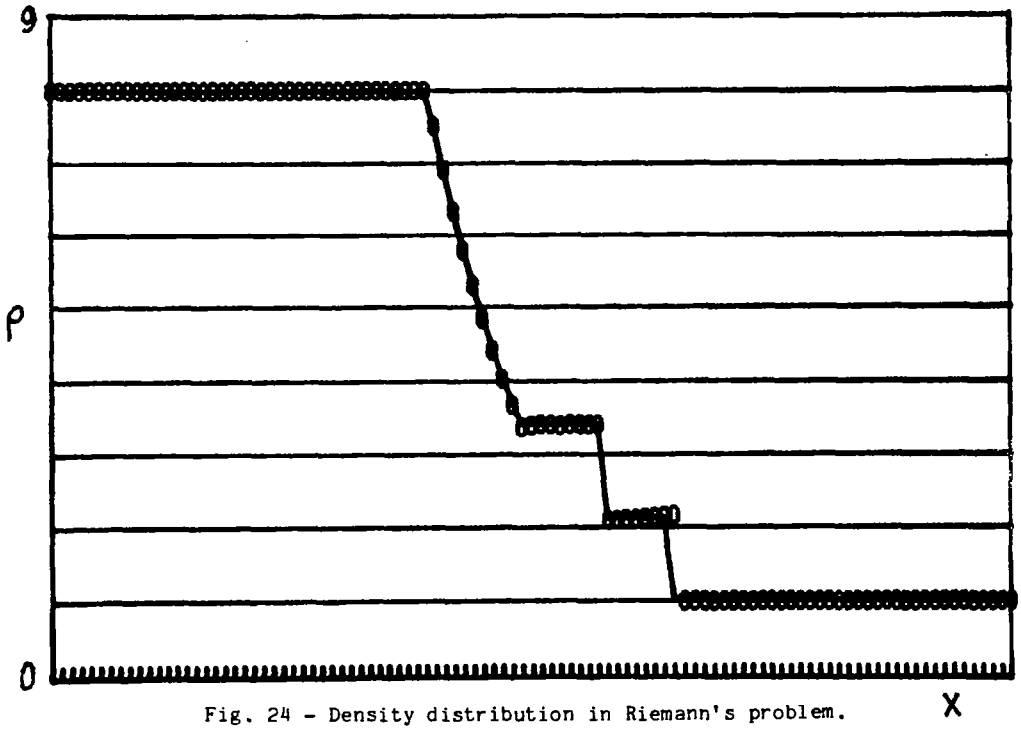

Fig. 24 - Density distribution in Riemann's problem.

within the interval at the time being plotted.

19. Merging of two shocks

When a shock overtakes another shock of the same family, the two merge into a single shock. A contact discontinuity and a weak, left-running expansion wave are generated (Fig. 27). The exact solution after the merger can be evaluated by the same procedure used for the collapse of an expansion shock and for the Riemann problem. We started with one shock having M=1.5 and the other having M=3. In run 401, we used 100 intervals. The main difficulty in this case stems from the narrowness of the expansion wave which, for a large number of computational steps, remains confined to a single interval. In addition, the "left-running" wave is actually moving from left to right, so that, when the wave front crosses over a mesh point, the point itself has to be returned to the unperturbed region. Results of our

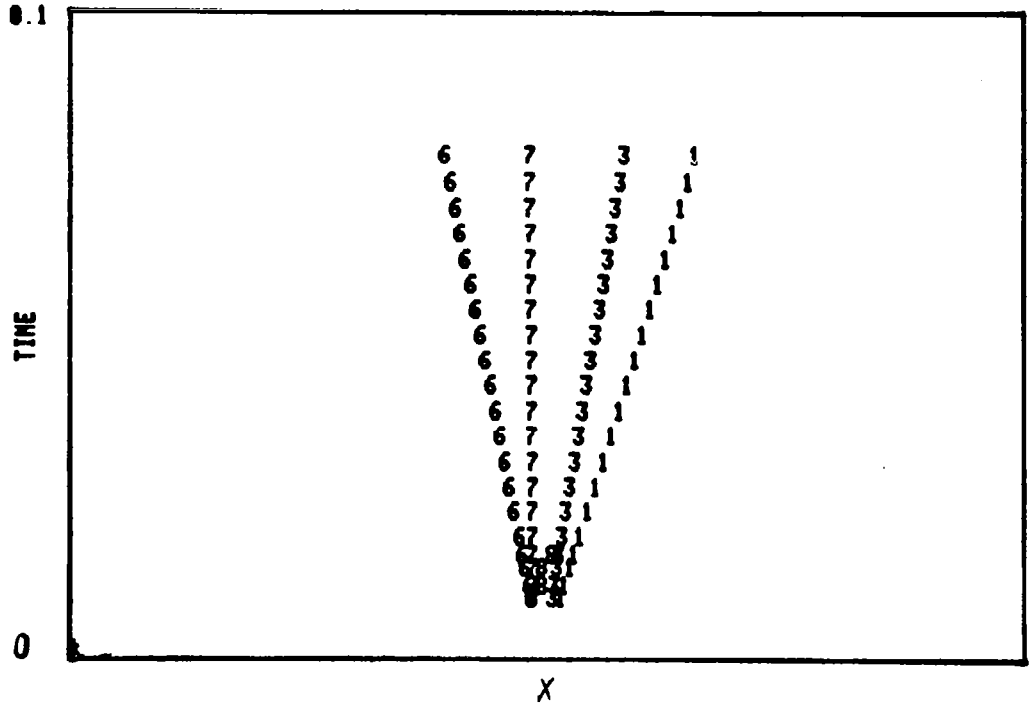

Fig. 25 - Tracking of discontinuities in Riemann's problem.

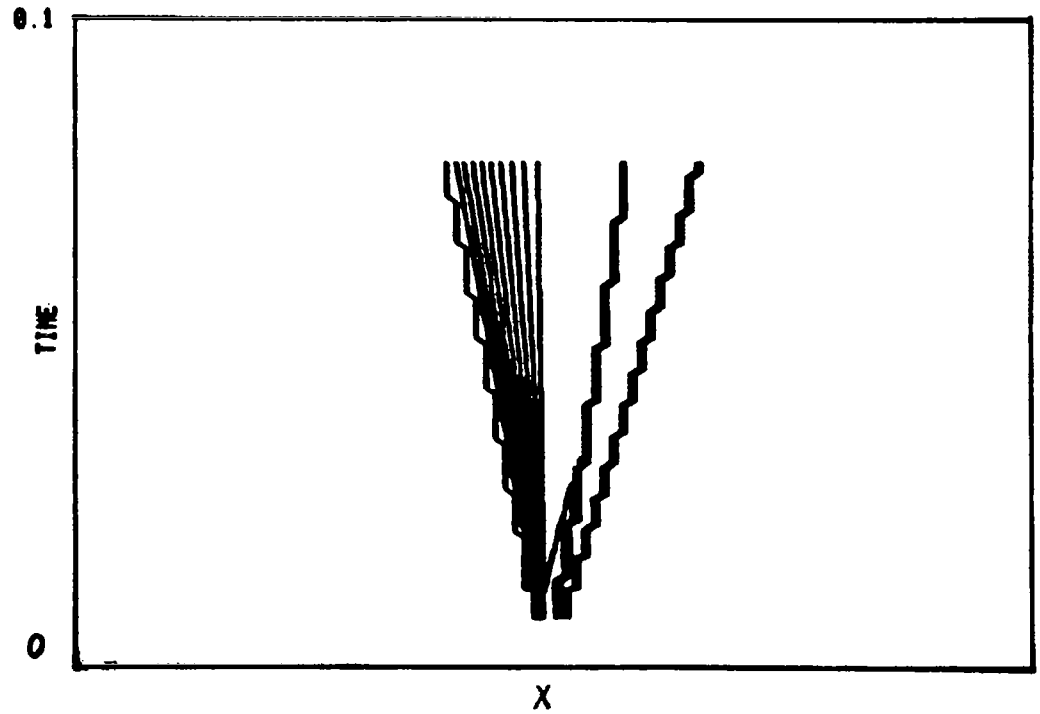

Fig. 26 - Isopycnics in Riemann's problem.

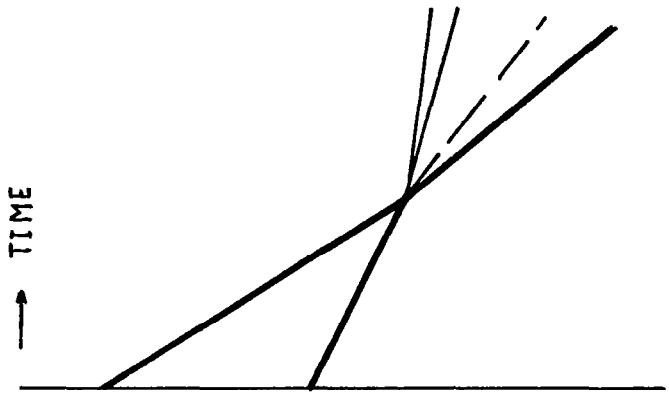

Fig. 27 - Merging of two shocks of the same family.

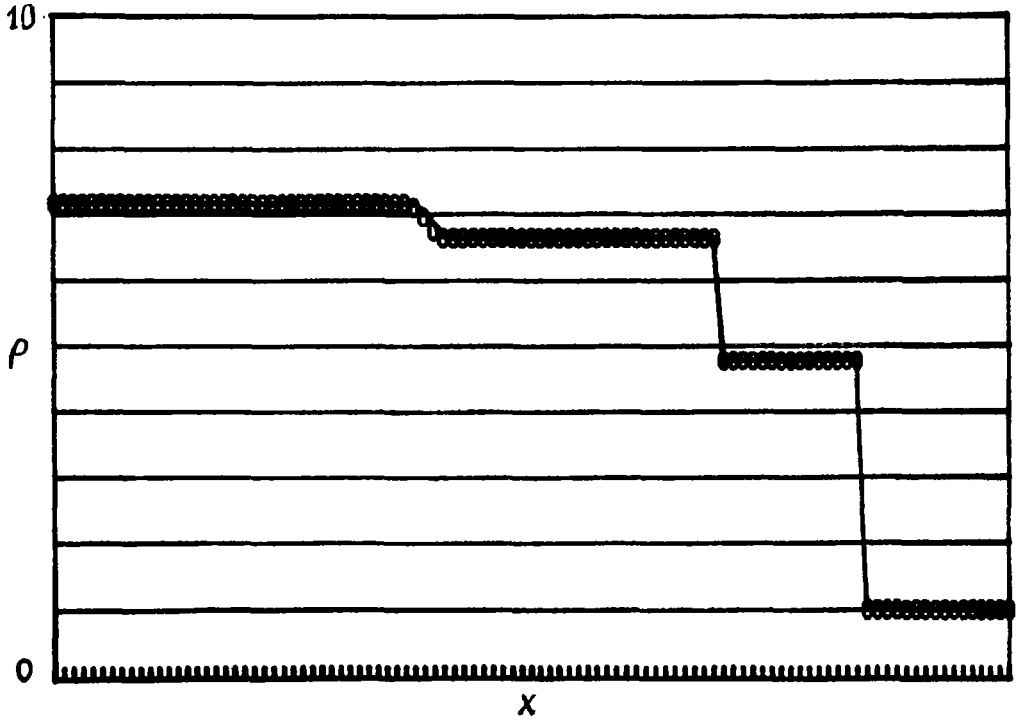

Fig. 28 - Density distribution in the merging of two shocks.

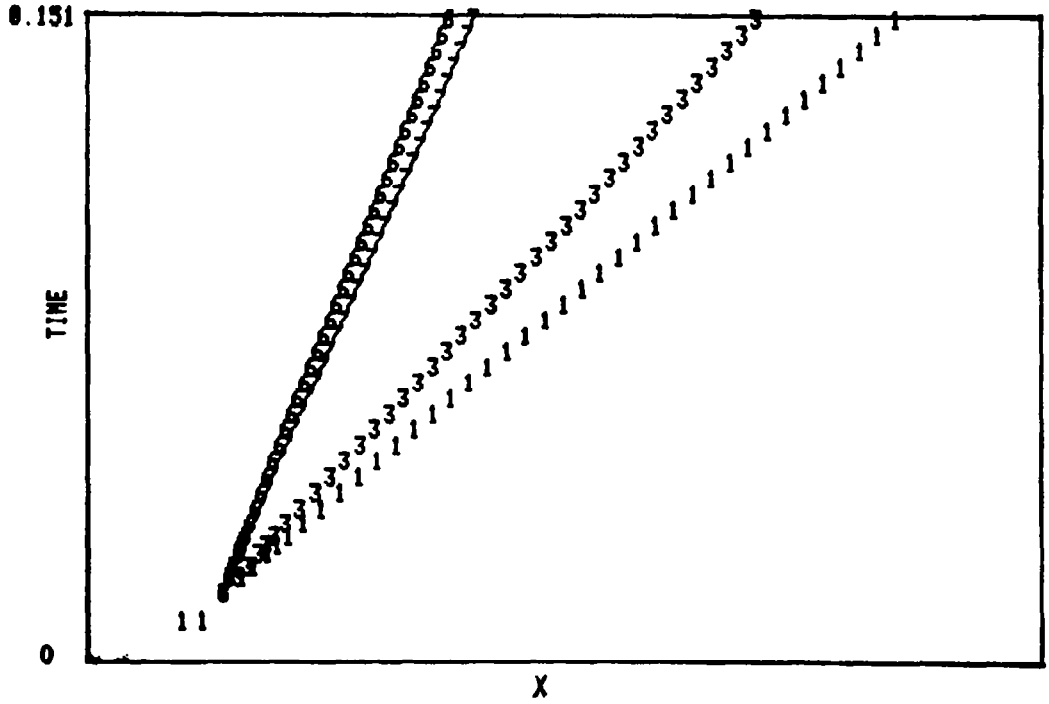

Fig. 29 - Tracking of discontinuities in merging of two shocks.

calculation are shown in Figs. 28 and 29. It is clear that, despite the difficulties just mentioned, the wave moves correctly and without smearing.

20. Decaying shock

A fixed shock separates a uniform, supersonic flow from a uniform, subsonic flow. A left-running expansion wave propagates through the subsonic region and interferes with the shock, which loses strength and moves downstream. No perturbation is propagated upstream of the shock, since the flow is supersonic in that region. Isopycnics are shown in Figs. 30 and 31 to demonstrate the effect of mesh size on accuracy.

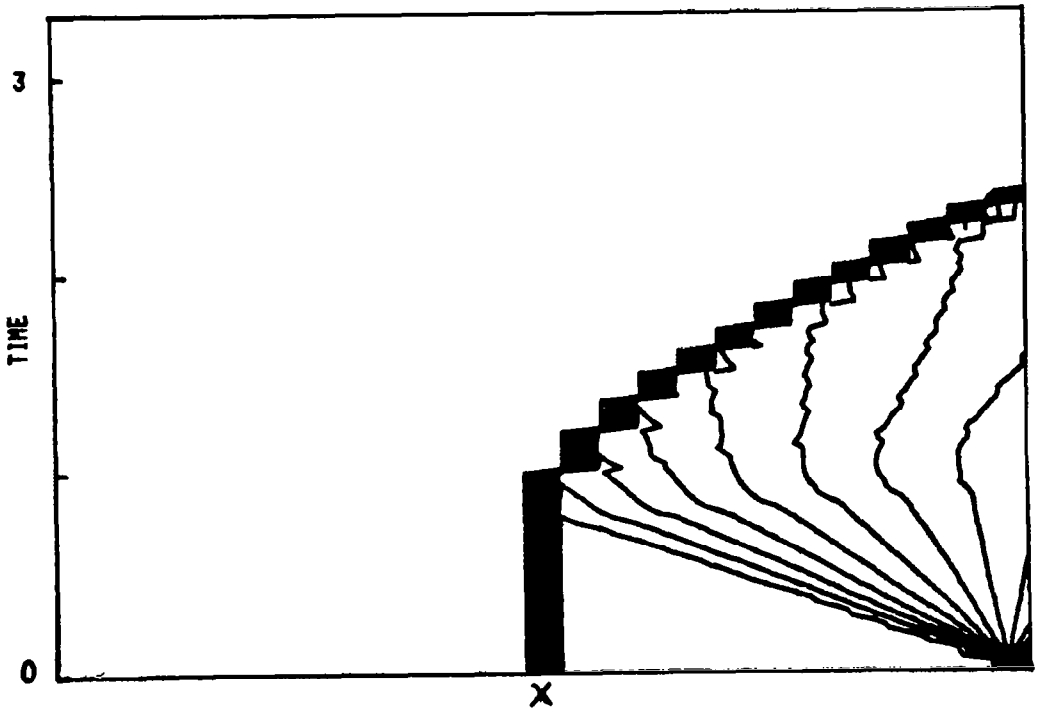

Fig. 30 - Isopycnics for a decaying shock, 25 intervals.

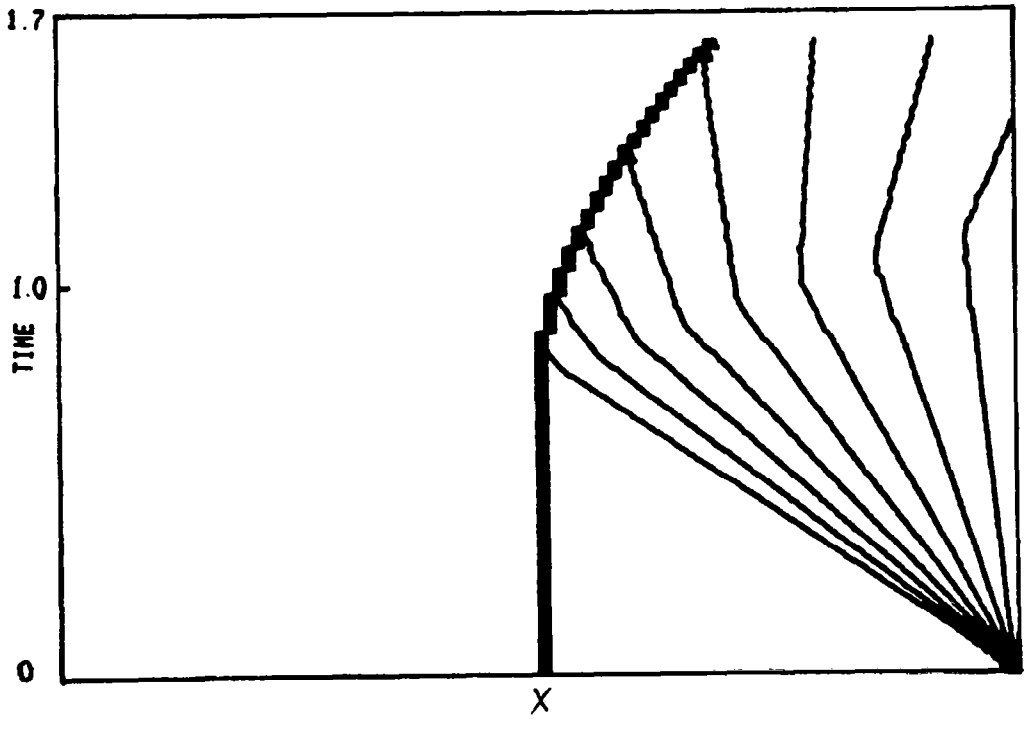

Fig. 31 - Isopycnics for a decaying shock, 50 intervals.

21. Interaction of a shock and a contact discontinuity

Two different flow patterns may be produced by the interaction of a shock and a contact discontinuity. If the shock penetrates into a region where the speed of sound is lower, the shock itself is refracted and another shock emerges, of the opposite family. A contact discontinuity is also produced. If the shock penetrates into a region where the speed of sound is higher, the shock is refracted and a centered expansion wave is produced, together with a contact discontinuity. The two cases are shown in Fig. 32.

We assume that the flow in regions 1,2, and 3 is given. In particular, we assume that $u_2=u_3=0$, $a_3=\gamma^{1/2}$, $p_2=p_3=1$, $s_3=0$; we prescribe a_2 and compute s_2 from

$$a_2/a_3 = \exp(\delta s_2)$$

We also prescribe the Mach number of the shock and obtain all pertinent values in region (1) as above.

In the first case ($a_2>a_3$), we find the exact solution by trial-and-error. The relation to be used, with W_{53} = velocity of the refracted shock, W_{14}= velocity of the reflected shock, are:

$$M_{53} = W_{53}/a_3$$

$$P_5 = \ln [(\gamma M_{53}^2 - \delta)/(1+\delta)]$$

$$u_5 = \frac{\gamma^{1/2}}{1+\delta} (M_{53} - 1/M_{53})$$

$$a_5 = [\gamma(\gamma M_{53}^2 - \delta)(1 + \delta M_{53}^2)]^{1/2} / [(1+\delta)M_{53}]$$

$$s_5 = [P_5 - \gamma \ln (1+\delta)M_{53}^2\gamma\delta$$

$$P_4 = P_5$$

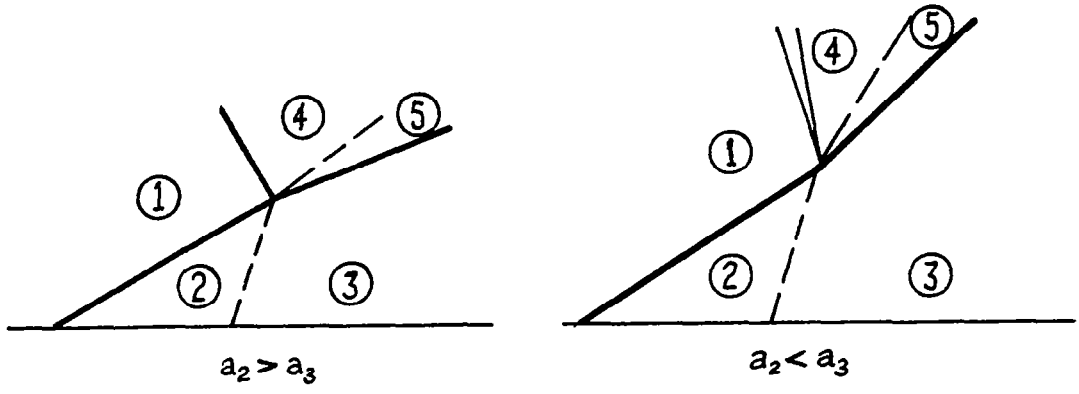

Fig. 32 - Interaction of a shock and a contact discontinuity.

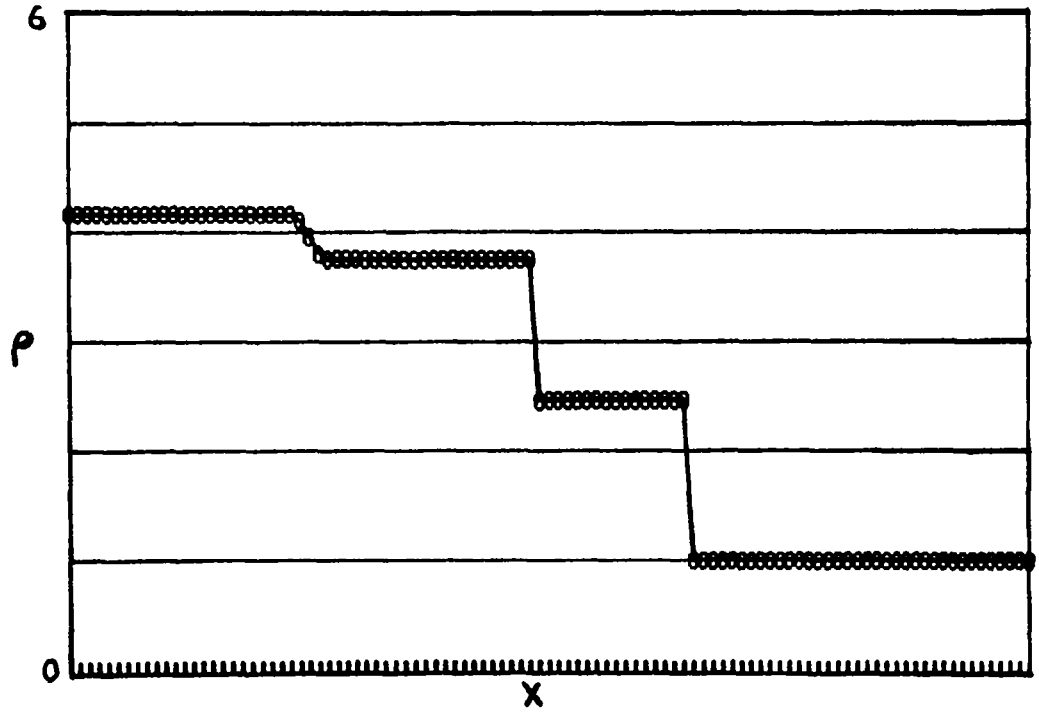

Fig. 33 - Density after shock-contact discontinuity interaction, second kind.

$$u_4 = u_5$$

$$P_4 = P_1 + \ln\left[(\gamma M_{14}^2 - \delta)/(1+\delta)\right]$$

$$W_{14} = u_1 - a_1 M_{14}$$

$$u'_4 = \left[u_1(1+\delta M_{14}^2) + W_{14}(M_{14}^2 - 1)\right] / \left[(1+\delta)M_{14}^2\right]$$

An error results from $u_4 - u'_4$ and must be made to vanish.

In the second case ($a_2 < a_3$), a similar procedure is followed. All the equations above are used again, except the last three, which must be replaced with:

$$s_4 = s_1$$

$$a_4 = a_1 - \delta(u_4 - u_1)$$

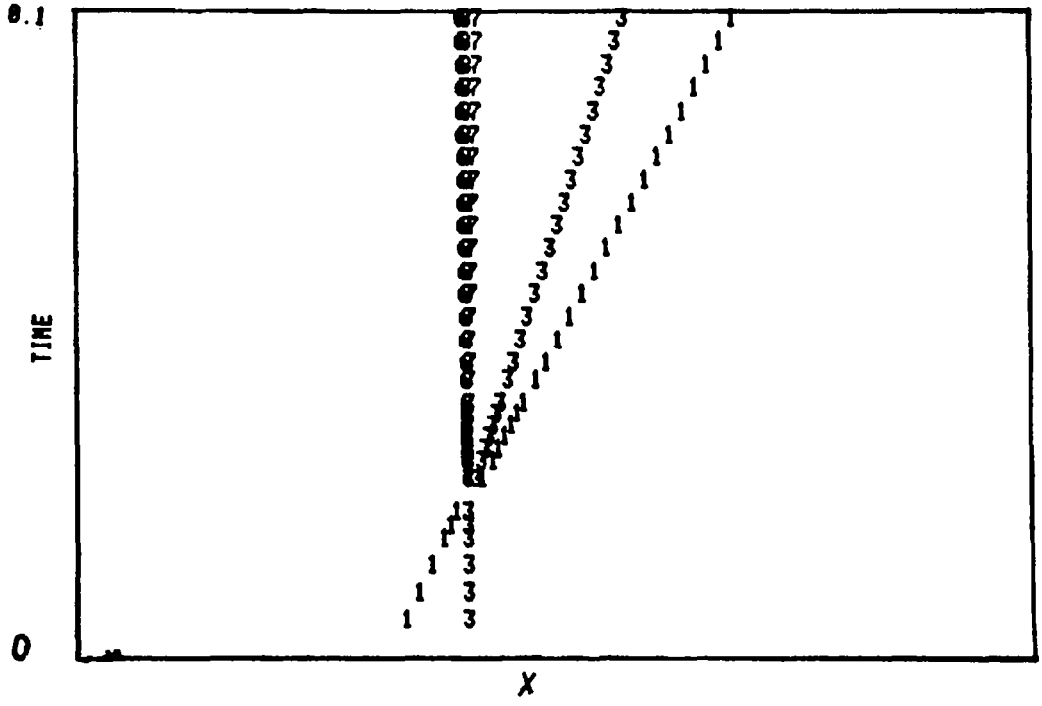

Fig. 34 - Tracking of discontinuities in shock-contact discontinuity interaction, second kind.

An error results from

$$a_4 - a_5 \exp[\delta(s_1 - s_5)]$$

and must be made to vanish.

In Figs. 33 and 34 we present the results of a calculated interaction of the second type. The shock Mach number is 2, the contact discontinuity is originally still, and the ratio of the speeds of sound between left and right hand side of the discontinuity is 0.8. Its most interesting feature is the perfect description of an extremely narrow expansion wave.

In Fig. 35 the result of a similar calculation, with a ratio of speeds of sound $a_2/a_3=4$, is presented. The pattern is now re-

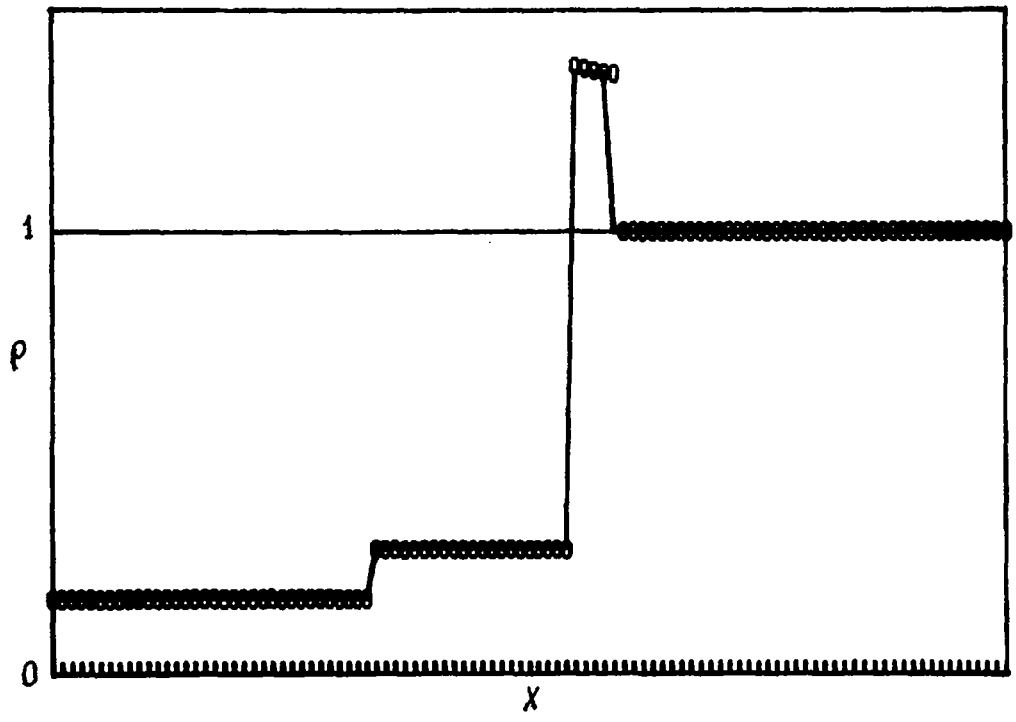

Fig. 35 - Density after shock-contact discontinuity interaction, first kind.

versed with respect to Fig. 33, and a weak shock is reflected.

22. Interaction of two expansion waves

At t=0, two centered expansion waves of opposite families are produced at x=0 and x=1. The one at the left is weaker than the one at the right. The first is, indeed, all subsonic and all contained in the (x>0)-region. The second has a supersonic part which does not appear in the (x<1)-region. Heads and tails of the waves are shown in Fig. 36, as computed between x=0 and x=1. Isopycnics are shown in Fig.37. They are symmetric up to the instant of interaction. The subsequent dissymmetry is a consequence of the different strengths of the waves. The top of Fig. 37 shows, on the left, the beginning of a new simple wave.

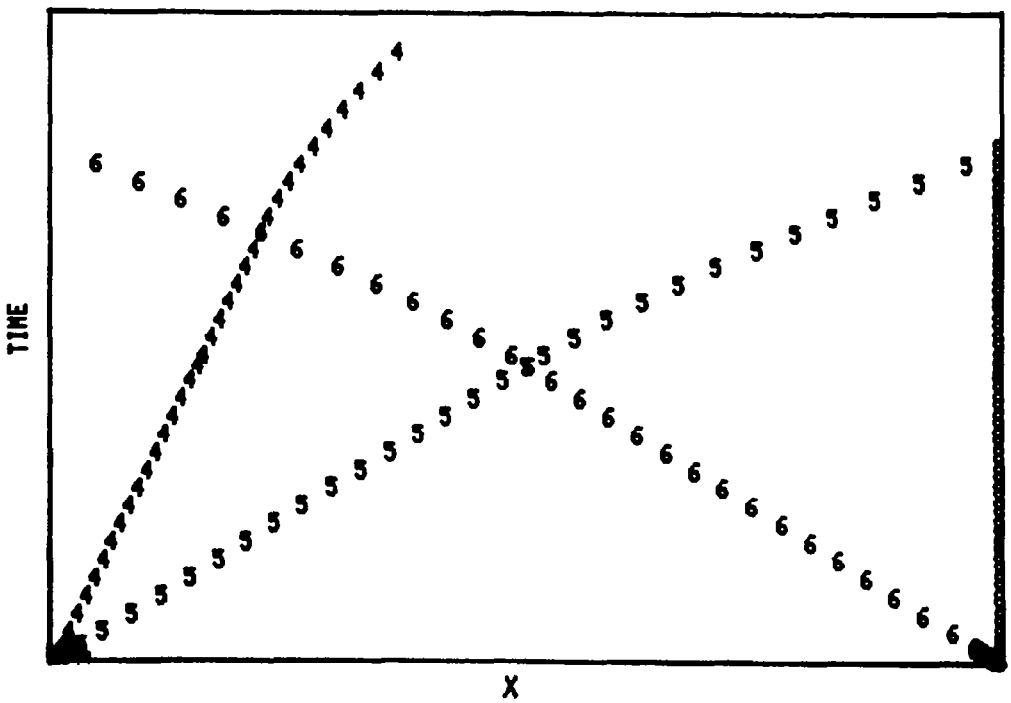

Fig. 36 - Tracking of discontinuities in expansion waves interaction.

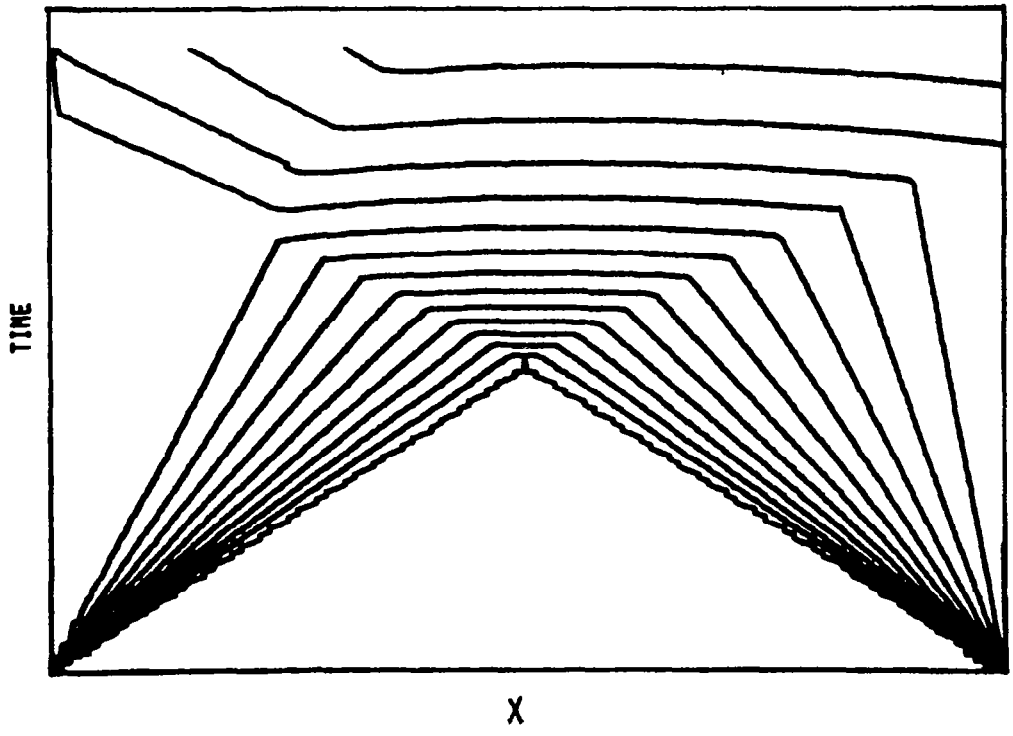

Fig. 37 - Isopycnics in the interaction of two expansion waves.

23. A more complicated pattern

To show the ability of the computational logic to handle a large number of discontinuities at the same time, and to take proper care of their interactions, we have considered the flow produced by the simultaneous breaking of two diaphragms. Initially, the flow appears as the succession of two similar patterns, of the type shown in Fig. 25. An interaction of the type shown in Fig. 31 is the first to occur, complicated by the motion of the flow behind the moving shock. A shock-contact discontinuity interaction will eventually occur but is not shown in the figure (Fig. 38). Isopycnics are shown in Fig. 39. The shock to the right is too weak to appear, since the number of level lines is automatically controlled by the program to avoid excessive clustering of lines.

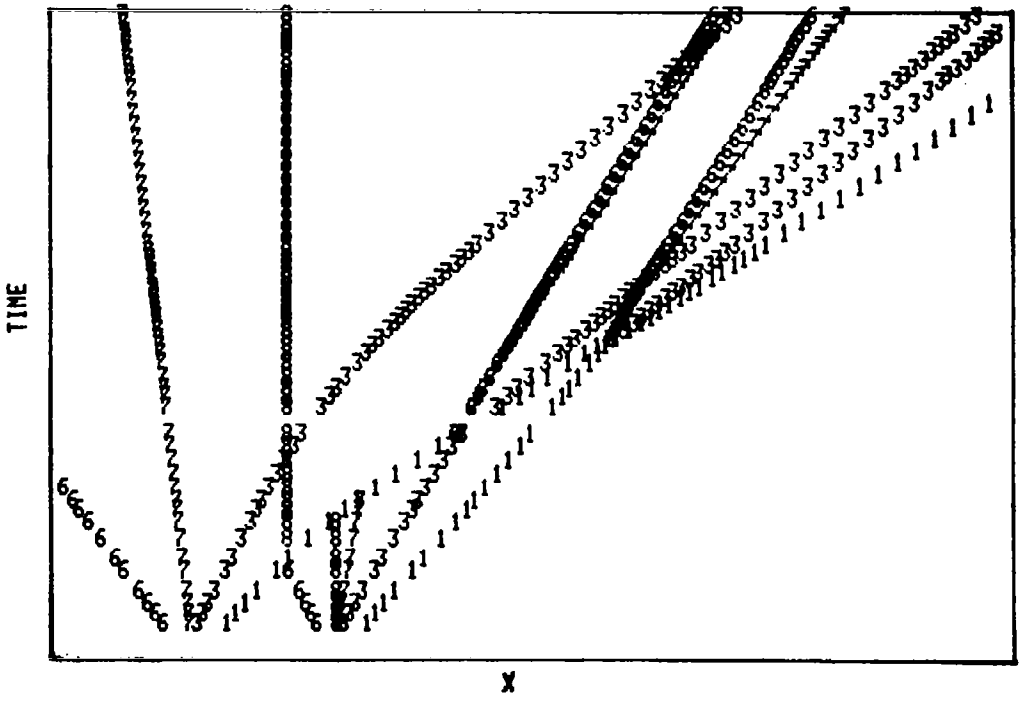

Fig. 38 - Tracking of discontinuities for two simultaneous Riemann problems.

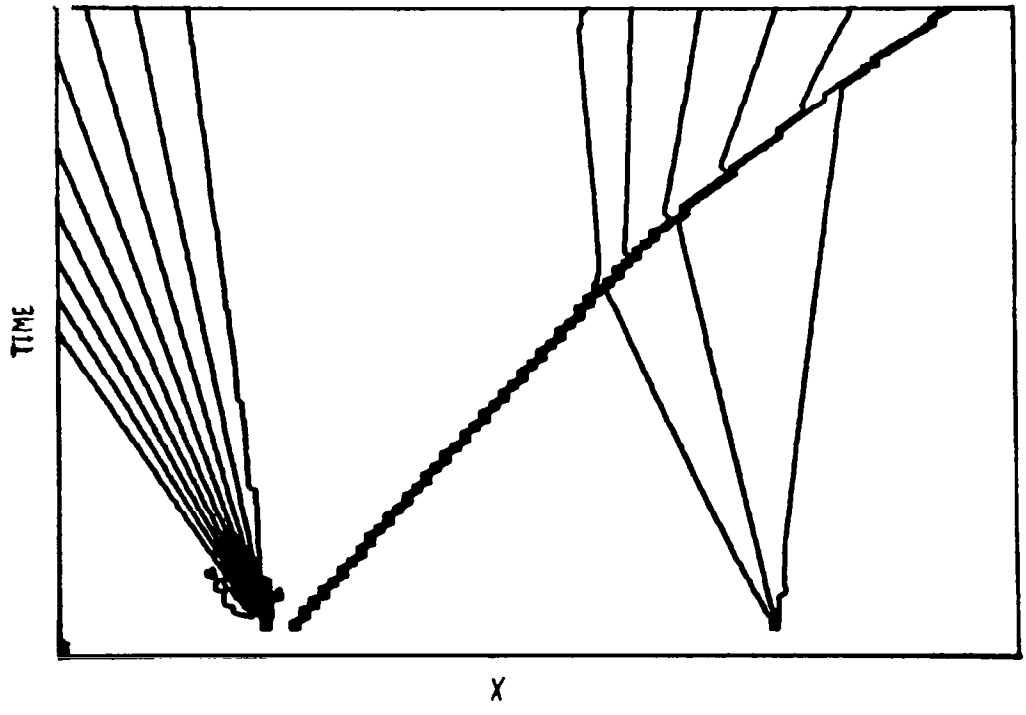

Fig. 39 - Isopycnics for two simultaneous Riemann problems.

24. Numerical exercises on gradient discontinuities

In Section 7, we have discussed the numerical problems related to the presence of gradient discontinuities, in general terms. The code described in Section 14 can be easily modified to delete the tracking of gradient discontinuities, in order to support our arguments with some quantitative experiments.

We begin considering a centered expansion wave originated at x=0.1682, t=-0.2804, by a piston moving backwards with a velocity equal to -0.6. The exact solution is computed at t=0 (note that in this case both a and u are linear within the wave, at a constant t). The computation is then started at t=0, using the λ-scheme as originally described in Section 5, at all points. The result is almost perfect (Fig. 40); the example does not suggest any need for special trackings or modifications to the scheme.

The same computation is repeated (Fig. 41) reducing the computational stepsize by a factor of 10. A precursor disturbance appears, although it is not large enough to be considered as a threat to the accuracy of the computation. Note that in Figs. 40 and 41 the speed of sound, not the density, is plotted; the results, however, are the same, qualitatively. This exercise is made to support our arguments in Section 5. It must be noted that, in a complicated flow, the stepsize may have to be drastically reduced at certain points, and all other points are affected; therefore, the possibility of dispersion of wave fronts due to low Courant numbers is not a remote one.

More drastic effects are shown in Figs. 42 and 43 (where density again is on the ordinate). Here, the expansion wave is centered at t=0, x=0 and the motion of the piston is so fast that the flow becomes sonic at the left boundary. The calculation performed with a tracking of the gradient discontinuity produces results which fall exactly on the solid line. Without tracking, the results show a sizeable precursor and a consequent degeneration over the entire wave (Fig. 42). The effect is, of course, enhanced when the stepsize is reduced by a factor of 10 (Fig.

43).

The next figure (Fig. 44) shows the result of the calculation of the same Riemann problem presented in Fig. 24. The deterioration of the expansion wave is evident and does not require any comment.

A similar deterioration appears in Fig. 45, which should be compared with Fig. 28. At the time considered in the figure, the expansion wave is barely encompassing four intervals. Without

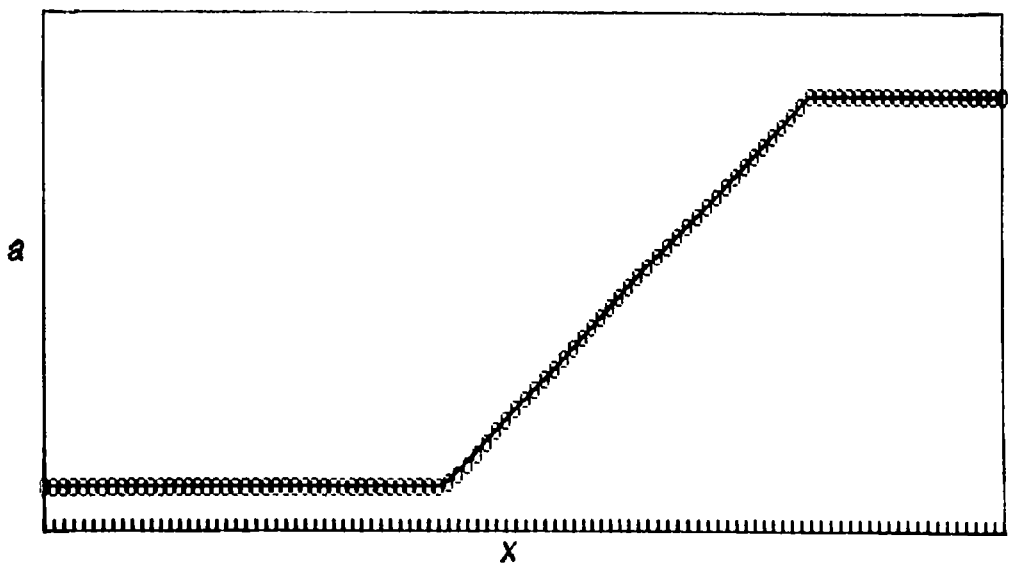

Fig. 40 - Speed of sound in a simple expansion wave, no tracking.

tracking, the wave is spread over 16 intervals.

25. More test cases. Quasi-one-dimensional flows

The following problems were considered as tests of the accuracy of the numerical analysis, rather than of the efficiency of the logic. To make the flow as far from uniform as possible, we consider ducts of variable cross-sectional area. The area, A(x), is defined by imposing a Mach number distribution between x=0 and x=1 and determining A(x) as satisfying the area-Mach number rela-

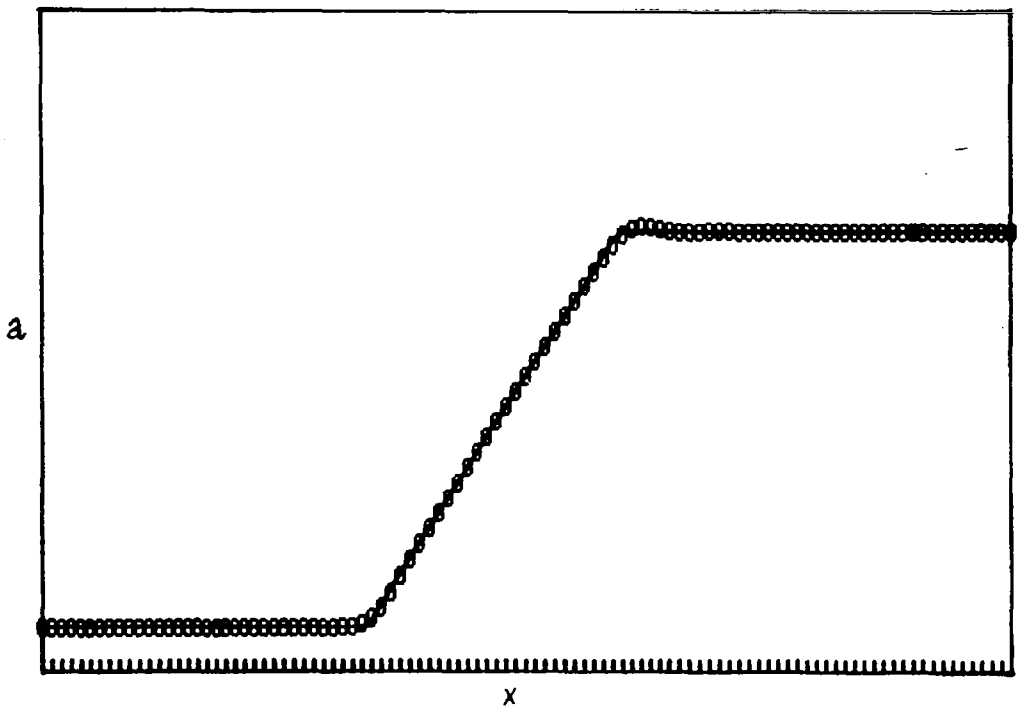

Fig. 41 - Speed of sound in a simple expansion wave, no tracking, reduced step size.

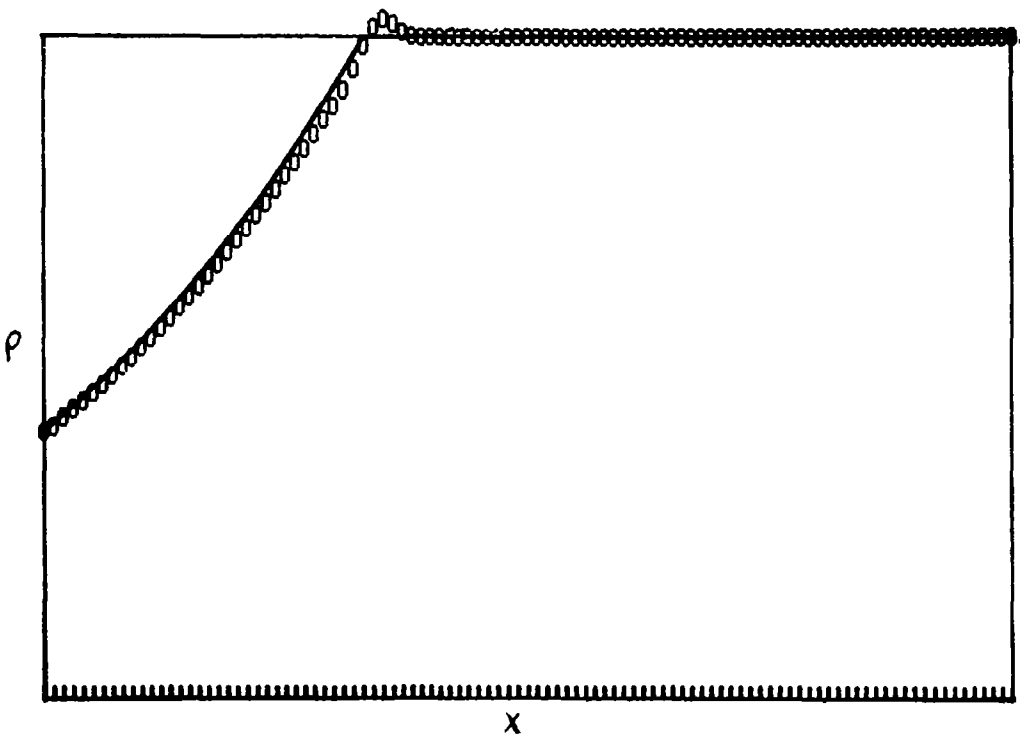

Fig. 42 - Density in a simple expansion wave, no tracking.

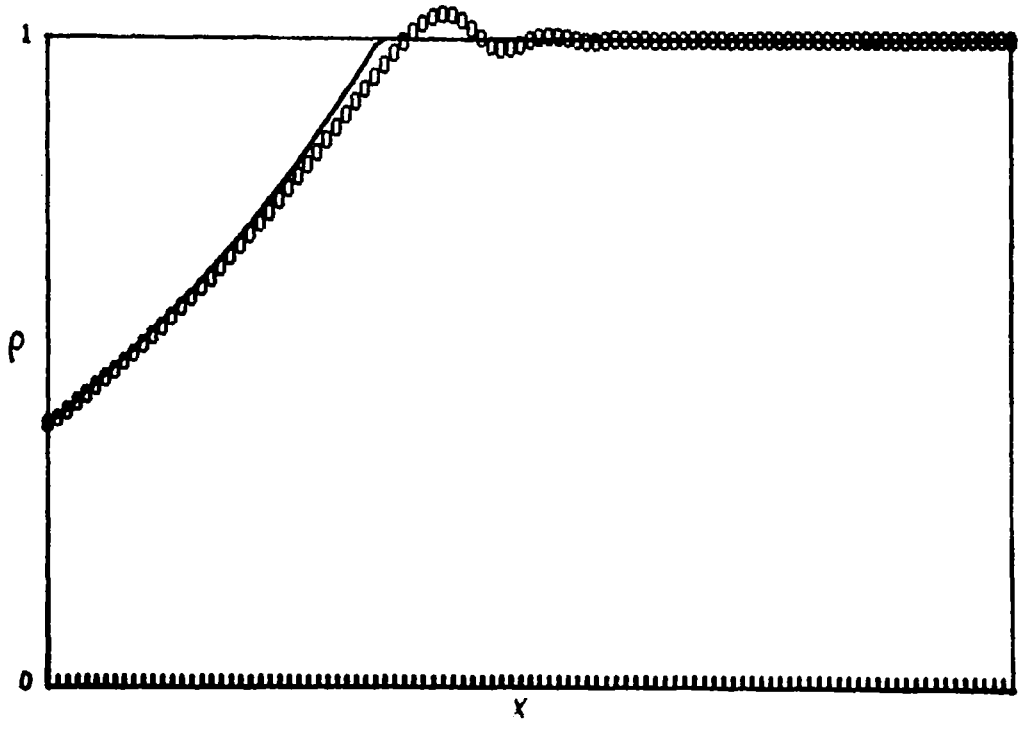

Fig. 43 - Density in a simple expansion wave, no tracking, reduced step size.

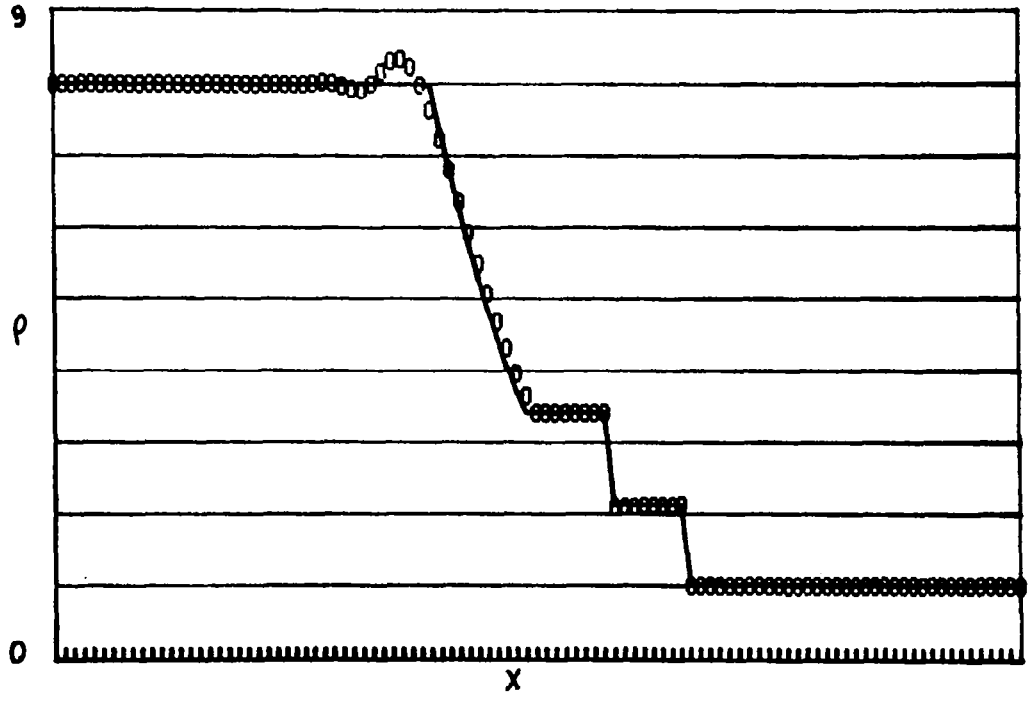

Fig. 44 - Density in Riemann's problem without tracking of gradient discontinuity.

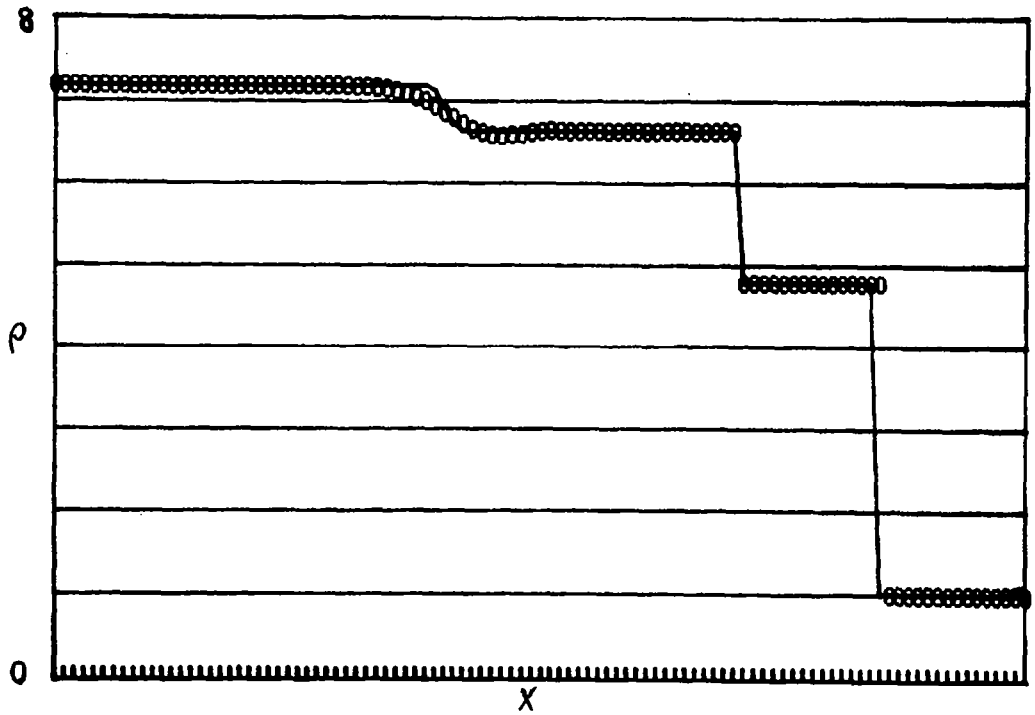

Fig. 45 - Density for merging shocks without tracking of gradient discontinuity.

tion for a steady, homentropic flow:

$$A = \frac{1}{M}\,(1 + \delta M^2)^{(1+\delta)/2\delta} \qquad (43)$$

In turn, the Mach number distribution is either linear (prescribed by the values of M at x=0 and x=1) or parabolic (prescribed by equal values of M at x=0, x =1 and by its value at x=1/2).

If we assume that the flow starts from a given initial state (for example, from rest, with a sudden drop in pressure at x=1), but that it remains homentropic, and that the duct proceeds from an infinite cavity containing a gas at rest, the flow inside the duct will approach a steady state asymptotically, whose Mach number distribution should be the same as the one initially chosen to define A(x). We have, thus, an asymptotic exact solution with which the computed flow may be compared.

If the original Mach number crosses from subsonic to supersonic, and the prescribed exit pressure is properly chosen, the asymptotic steady state will no longer be homentropic. A steady

shock will appear in the divergent part of the duct, followed by a subsonic region. Once more, we have at our disposal the exact solution, which is easily obtained by prescribing the shock location and calculating the jump in the critical area. From the shock to the exit, M can be computed from (43), altering A by a constant factor. It will also be easy to find which exit pressure must be prescribed, consistent with a given shock location.

26. Subsonic, homentropic flows

1) If M is prescribed to go from 0.2 to 0.8 linearly (converging duct), an asymptotic steady state is reached very rapidly. If the distribution is the opposite one (diverging duct), it takes much longer to reach a steady state. These well-known facts are confirmed by the isopycnics of the two flows (Figs. 46

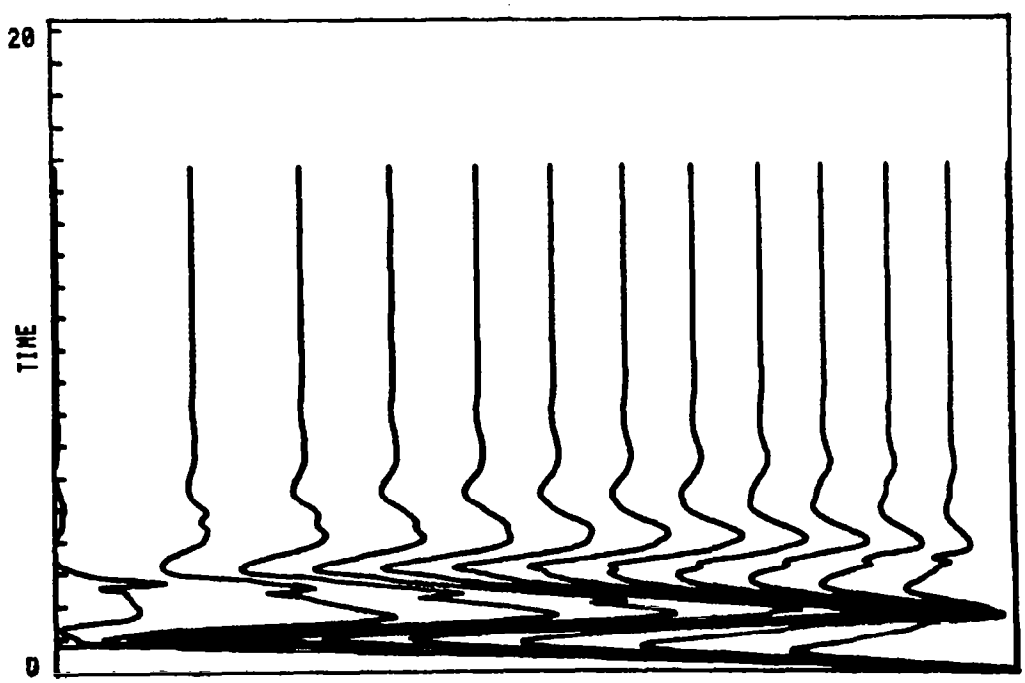

Fig. 46 - Isopycnics for converging duct.

and 47). The obvious steady state results are not worth showing.

2) If M is prescribed as a parabolic curve, with entry and exit values equal to 0.3 and a maximum value equal to 0.8, the isopycnic plot appears as in Fig. 48 and the asymptotic values

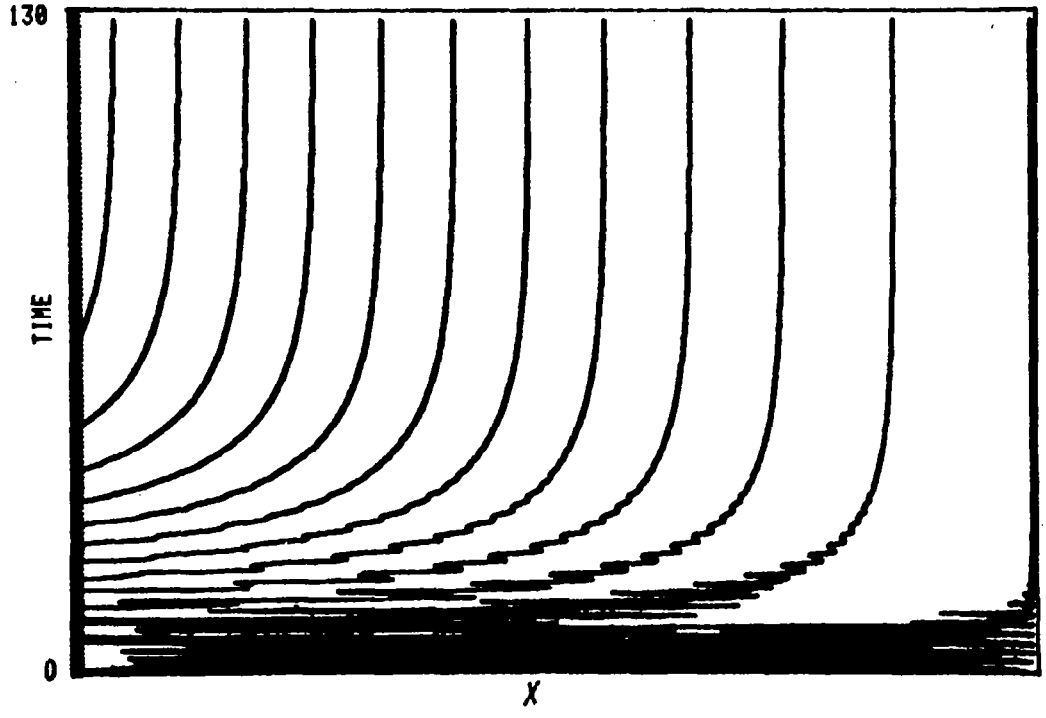

Fig. 47 - Isopycnics for diverging duct.

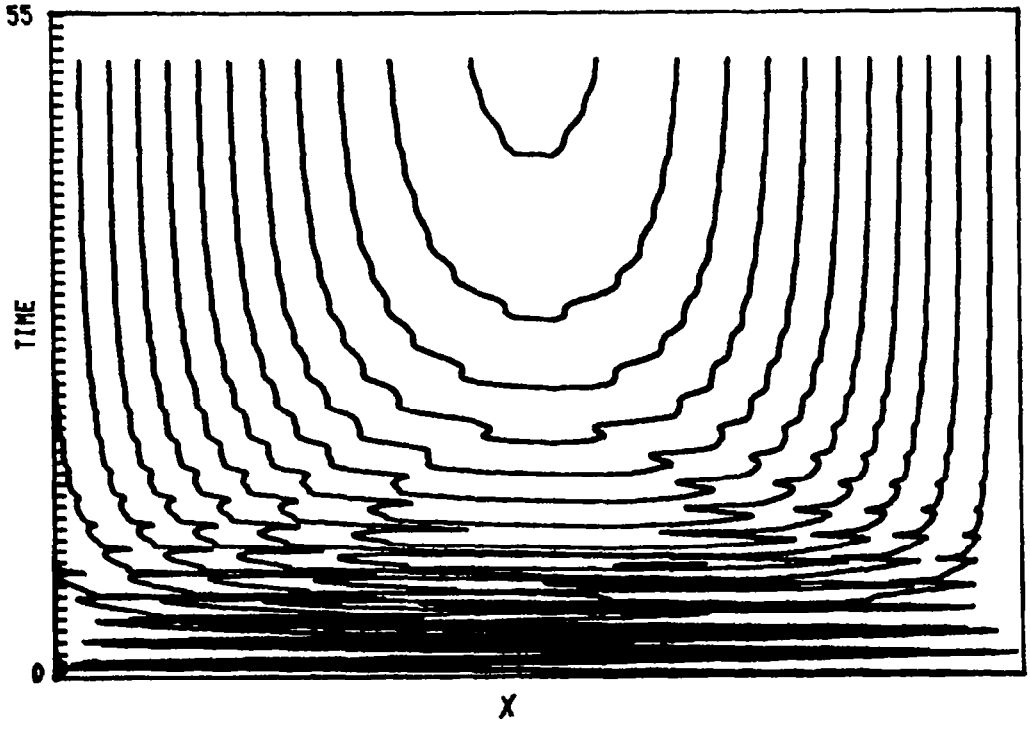

Fig. 48 - Isopycnics for parabolic duct.

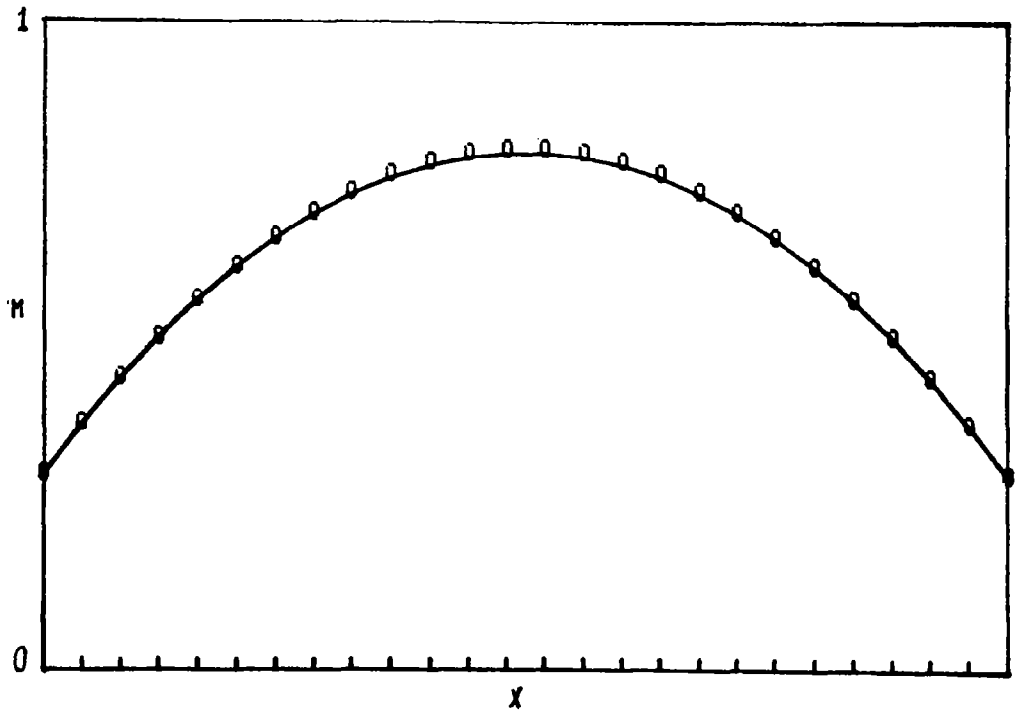

Fig. 49 - Steady state M(x) for parabolic duct, 0.3<M<0.8.

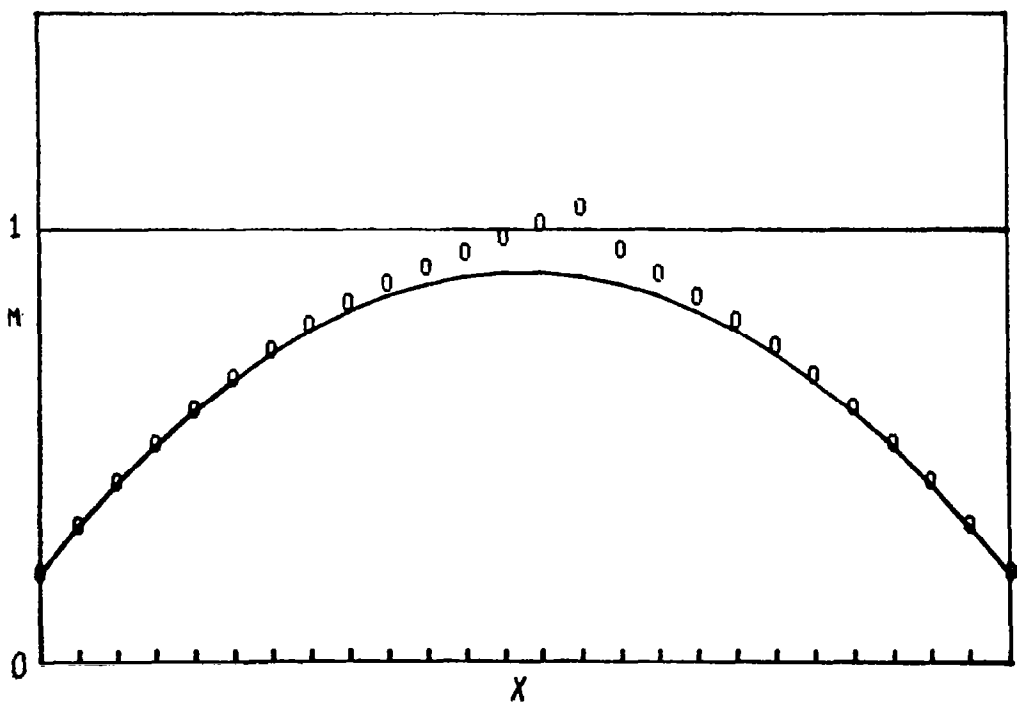

Fig. 50 - Steady state M(x) for parabolic duct, 0.2<M<0.9.

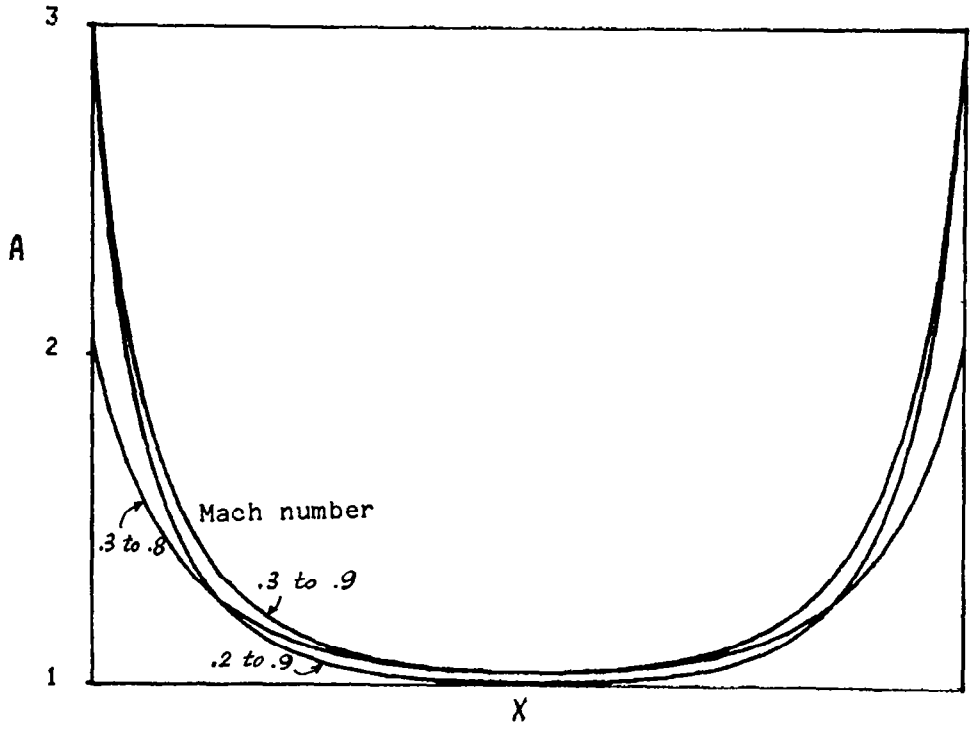

Fig. 51 - Area distributions in parabolic ducts.

(denoted by 0's) fall very well on top of the exact steady state solution (solid line, in Fig. 49).

Difficulties appear if the lower value of M is 0.2 instead of 0.3 and the upper value is 0.9 instead of 0.8. When starting from rest, after an initial phase in which the computed values become very close to the steady state solution, a second phase follows with some drifting in the upper subsonic region; eventually, the computed flow develops a small supersonic region, followed by a weak shock (Fig. 50). The failure of the code, which, at a first sight, could be attributed to lack of accuracy in the transonic region, is to be found in a lack of accuracy in the entry portion of the duct. The curve of A(x) in this case appears as shown in Fig. 51; for comparison, A(x) is also shown for the preceding case, $0.3 < M < 0.8$, and for the case, $0.3 < M < 0.9$. It seems that a quasi-one-dimensional approach is, in the present instance, inadequate to approximate the real behavior of a flow in a duct whose cross-sectional area varies so rapidly. Numerical errors in the calculation of the entry point may produce a slight error in stagnation enthalpy and a consequent change in

the critical area. In addition, the cross-sectional area remains flat and very close to 1 over a large portion of the duct; therefore, the change in the critical area may be sufficient to replace the prescribed duct with a duct having a throat exactly at x=0.5. The Mach number distribution shown in Fig. 50 is indeed consistent with such a geometry. Any other Mach number distribution generating channels without such a steep area distribution can be computed with accuracy. It is interesting to note that all these computations with parabolic Mach number distributions are extremely long, because the initial perturbation is very small and it requires a large number of waves, travelling back and forth along the channel, in order to produce a fast flow in the middle of it.

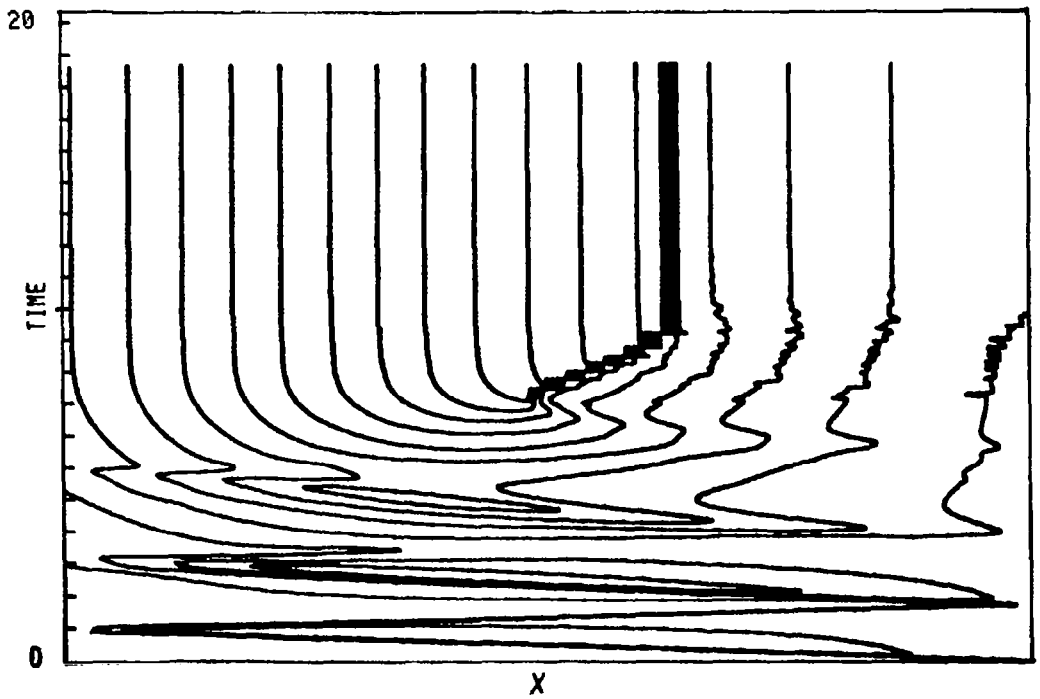

Fig. 52 - Isopycnics in Laval nozzle with a shock.

27. Transonic flows with a shock

We present in Figs. 52, 53 and 54 the results obtained by prescribing a duct geometry consistent with an isentropic linear Mach number distribution between M=0.5 and M=2.0, and an exit pressure consistent with the presence of a shock at x=0.63. As

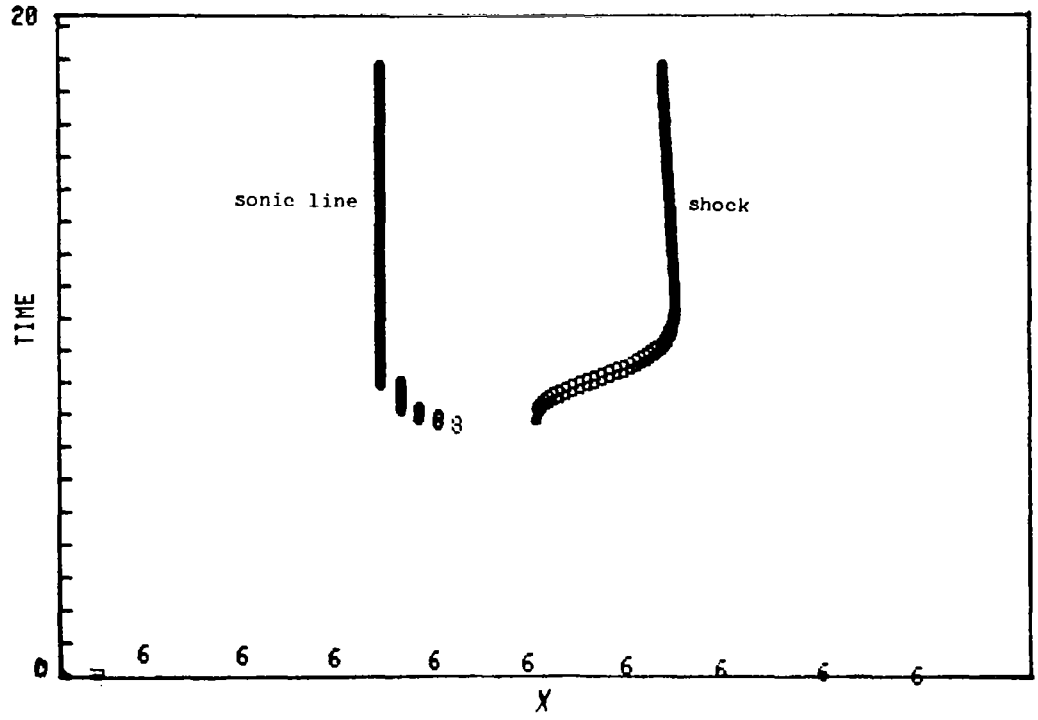

Fig. 53 - Tracking of sonic line and shock in Laval nozzle.

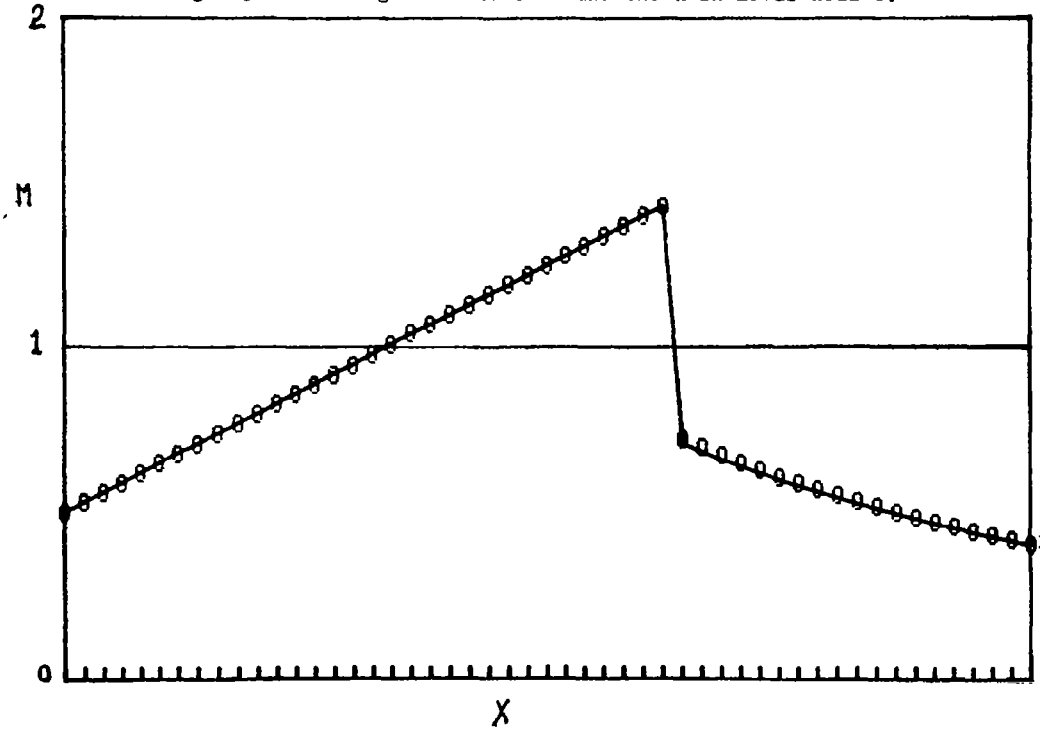

Fig. 54 - Steady state M(x) in Laval nozzle.

in the preceding cases, the flow is generated by the sudden drop of the exit pressure to the final value, the flow being originally at rest. The isopycnic plot clearly reveals the original receding expansion wave and its reflection as a compression wave, which eventually coalesces into a shock.

Finally, Fig. 55 shows the isopycnic pattern in the same duct, assuming that, for $t<0$, the flow in the duct was steady, with a shock somewhere between $x=0.63$ and $x=1$. At $t=0$ the exit pressure is suddenly lifted to the value of the previous case. The shock is pushed backwards to the new stable position, $x=0.63$. The final Mach number distribution is not shown, being the same as in Fig. 54.

28. An exercise on contact discontinuities

To conclude our numerical experiments, we present calculations made on two flows in a parabolic nozzle. In both cases, the flows start from rest. The initial entropy, however, is not constant. It is prescribed to be equal to 0 to the left of the throat and to have another value, $s_2 = (\ln\beta)/\delta$ to the right of it. The speed of sound equals $\gamma^{1/2}$ and $\beta\gamma^{1/2}$ at the left and right of the throat, respectively. If the speed of sound at the exit is dropped to a fraction, α, of its original value, a flow is generated and the contact discontinuity eventually moves throughout the divergent portion of the duct and exits from it. At a certain stage of the evolution, according to the value of β, the contact discontinuity may separate a subsonic flow from a supersonic flow, or vice versa. The case of $\alpha=0.7$, $\beta=1.2$ is shown in Figs. 56, 57 and 58, the case of $\alpha=0.7$, $\beta=0.7$ in Figs. 59, 60 and 61. A history of the evolution of the Mach number is depicted in Figs. 56 and 59, to show how the transonic transition occurs. The purpose of these calculations is to show that no symptoms of errors appear, regardless of the nature of the transition.

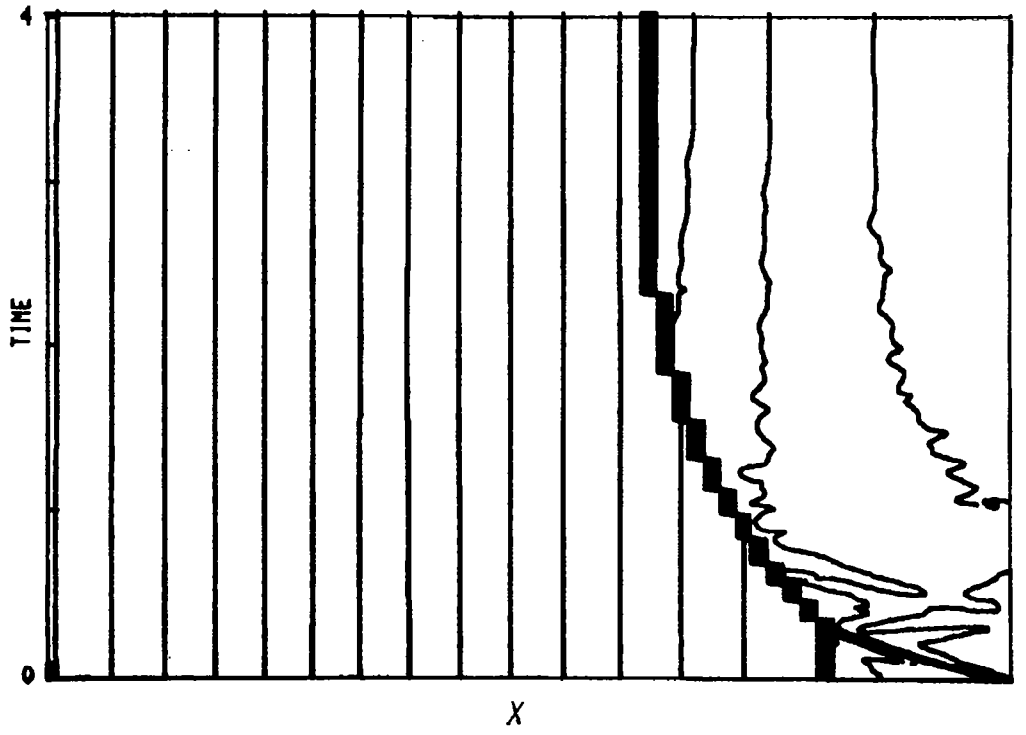

Fig. 55 - Isopycnics in Laval nozzle.

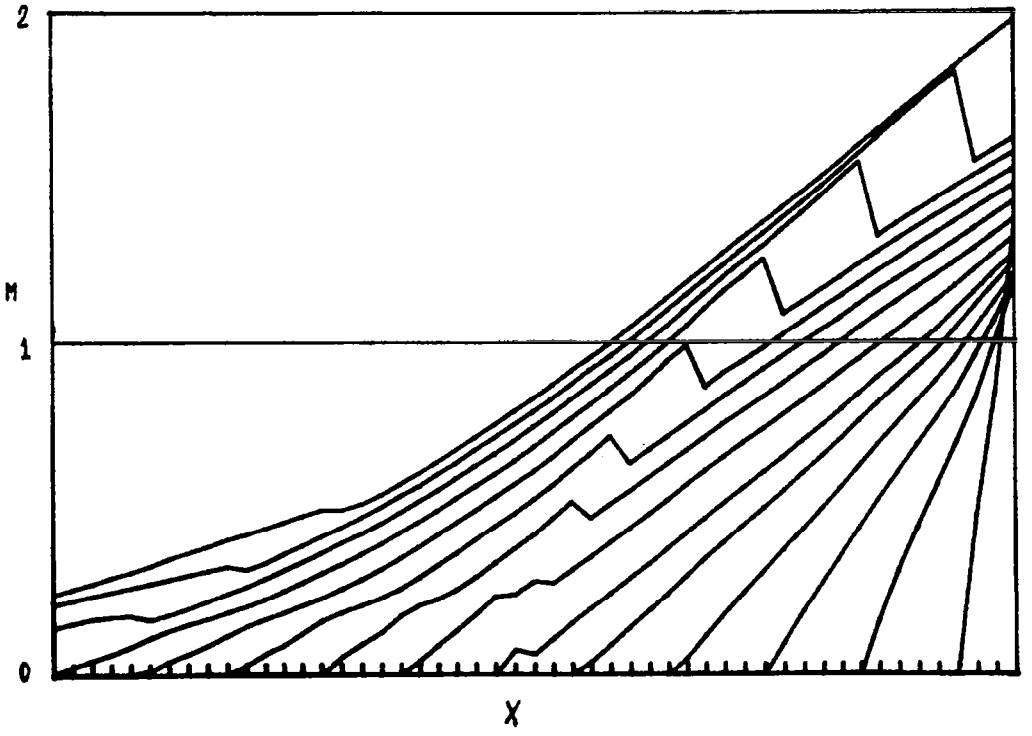

Fig. 56 - Evolution of M(x) in nozzle with contact discontinuity, $a_2 > a_1$.

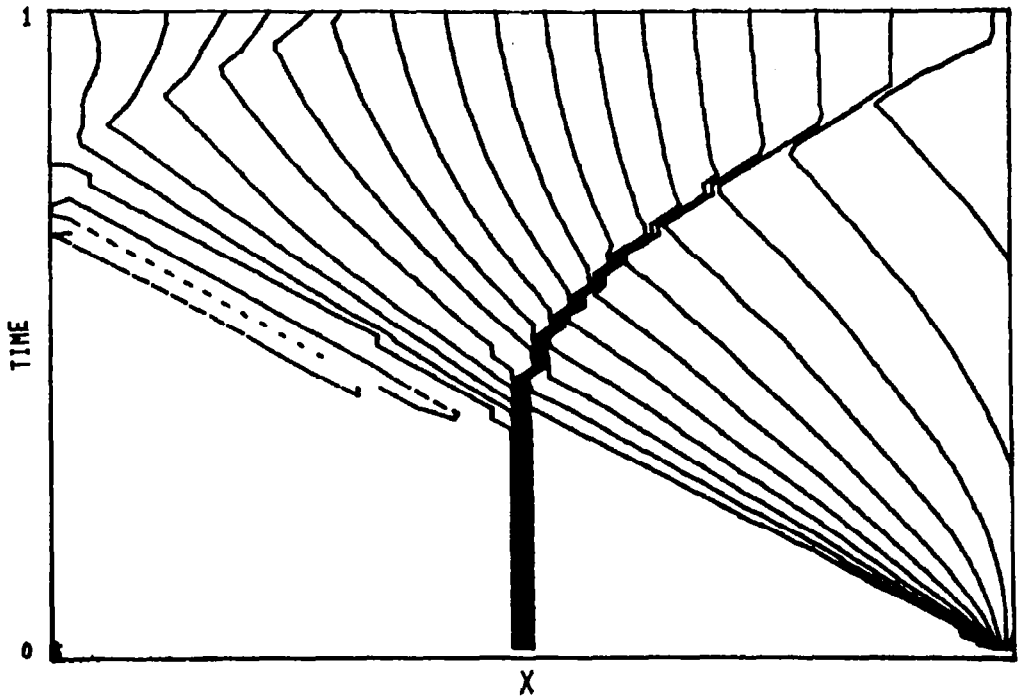

Fig. 57 - Isopycnics in nozzle with contact discontinuity, $a_2 > a_1$.

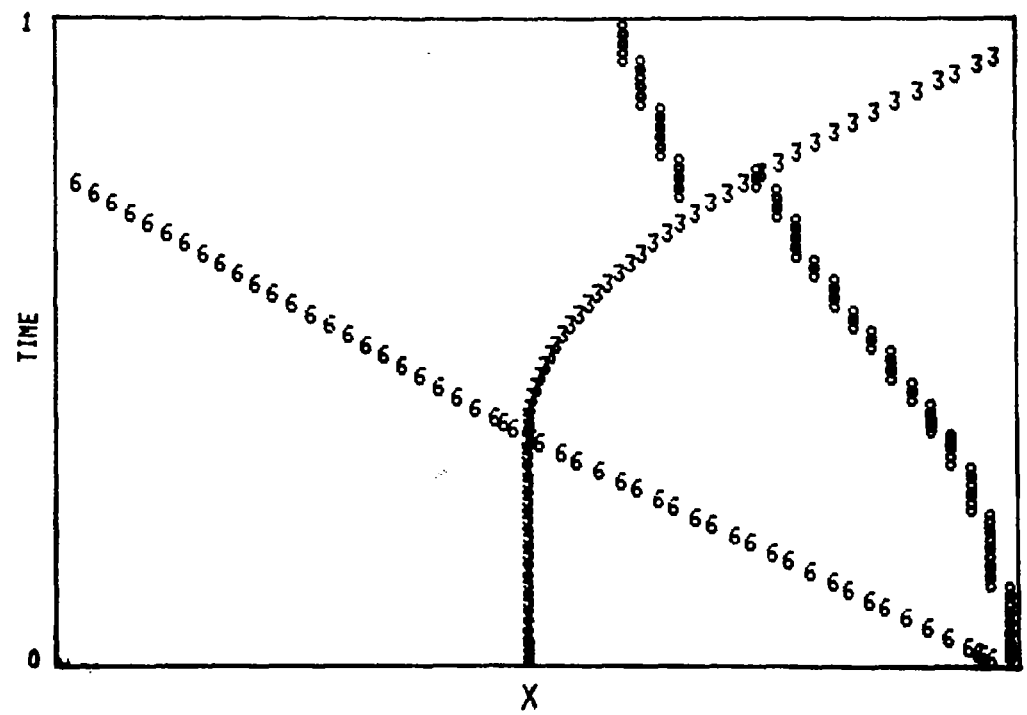

Fig. 58 - Tracking of discontinuities in nozzle, $a_2 > a_1$.

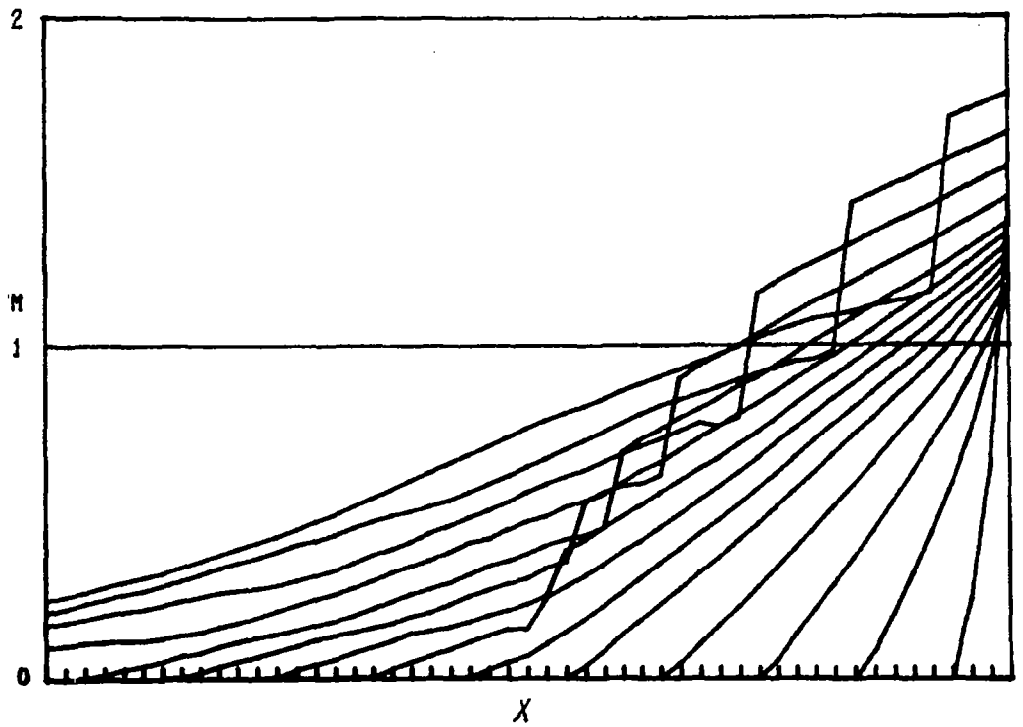

Fig. 59 - Evolution of M(x) in nozzle with contact discontinuity, $a_2<a_1$.

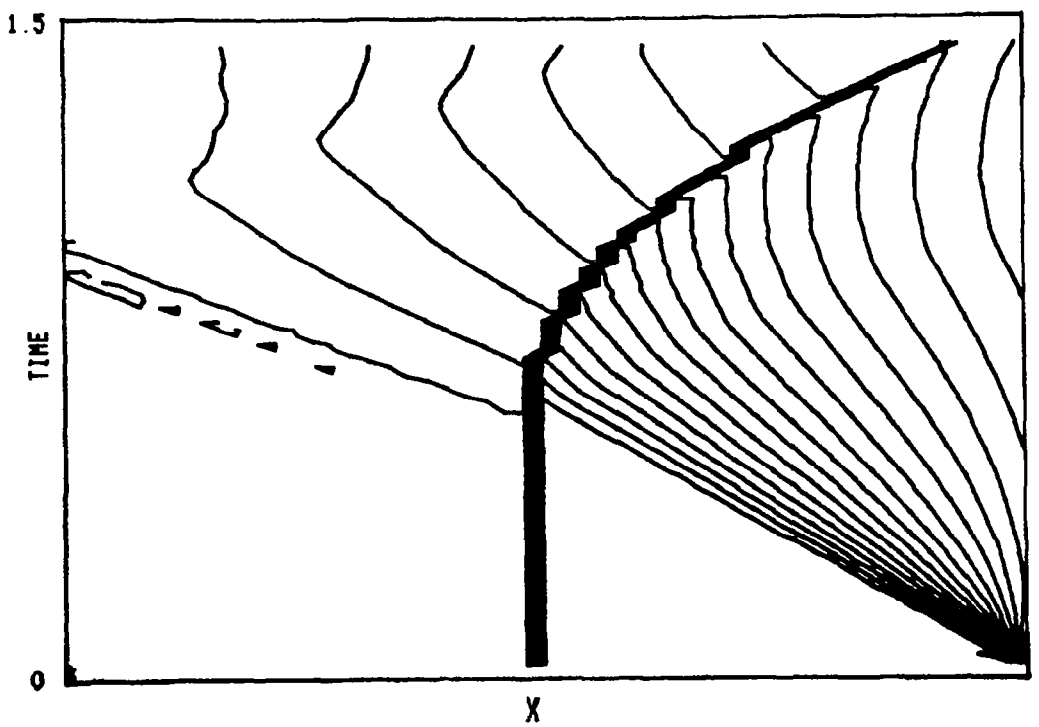

Fig. 60 - Isopycnics in nozzle with contact discontinuity, $a_2<a_1$.

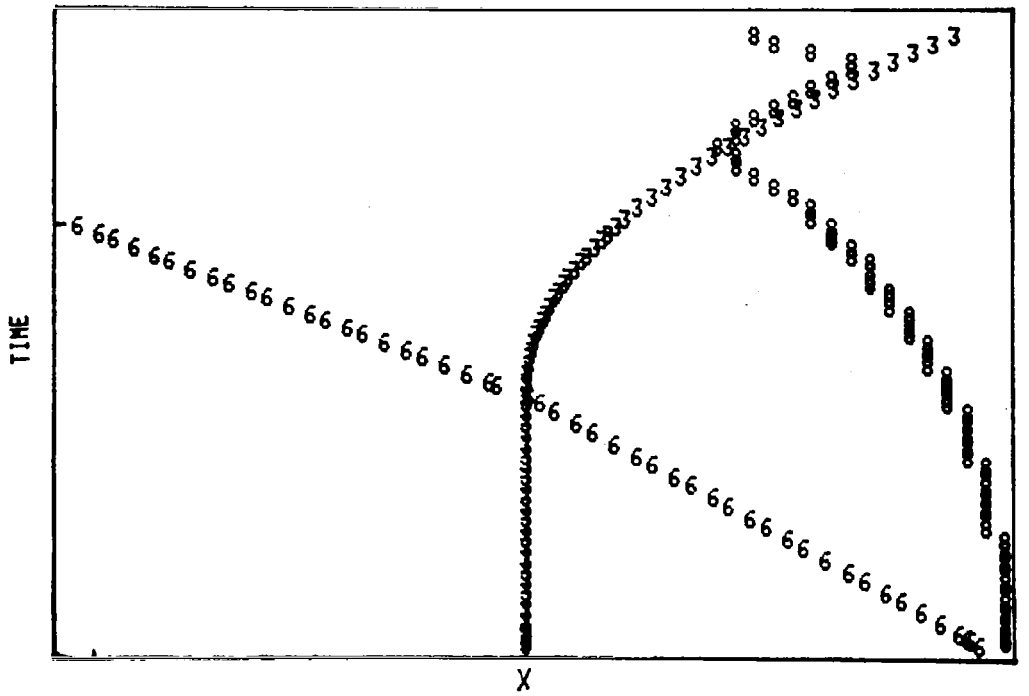

Fig. 61 - Tracking of discontinuities in nozzle, $a_2 < a_1$.

Concluding remarks

An improved method for the calculation of one-dimensional flows has been presented. It combines a simple and efficient version of the λ-scheme with tracking of discontinuities. The latter is needed to identify points where minor departures from the basic integration scheme are applied to prevent infiltration of numerical errors. Such a tracking is obtained via a systematic application of Boolean algebra. It is, therefore, very efficient. Fifteen examples of flow computations have been presented and discussed in detail. The results are exceptionally good. All discontinuities are captured within one mesh interval. Efforts are currently being made to extend the method to multidimensional flows.

References

1. Courant, R.; Isaacson, E. and Rees, M.: On the solution of nonlinear hyperbolic differential equations by finite differences. Comm.pure appl.Math. 5, 243-249 (1952).

2. Godunov, S.K.: Finite difference method for numerical computation of discontinuous solutions of the equations of fluid dynamics. Mat. Sb. 47, 271-306 (1959).

3. Taylor, T.; Ndefo, E. and Masson, B.S.: A study of numerical methods for solving viscous and inviscid flow problems. J.Comp.Phys. 9, 99-119 (1972).

4. Steger, J.L. and Warming, R.F.: Flux vector splitting of the inviscid gasdynamic equations, J.Comp.Phys. 40, 263-293 (1981).

5. Roe, P.L.: Approximate Riemann solvers, parameter vectors and difference schemes. J.Comp.Phys. 43, 357-372 (1981).

6. van Leer, B.: Towards the ultimate conservative difference scheme, IV. A new approach to numerical convection. J.Comp.Phys. 23, 276-299 (1977).

7. Engquist, B. and Osher, S.: One-sided difference approximations for nonlinear conservation laws. Math.Comp. 36, 321-351 (1981).

8. Moretti, G.: The lambda-scheme. Comp. and Fl. 7, 191-205 (1979).

9. Pandolfi, M.: A contribution to the numerical prediction of unsteady flows. Accepted for publication - AIAA Paper 83-0121 (1983).

10. Zhu, Y-l and Chen, B-m: Difference methods for initial-boundary-value problems and computation of flow around bodies. Comp. and Fl. 9, 339-364 (1981).

11. Moretti, G. and Zannetti, L.: A new, improved computational technique for two-dimensional unsteady compressible flows. AIAA Paper 82-0168 (1982).

12. Zhong, X-c and Moretti, G.: Comparison of different integration schemes based on the concept of characteristics as applied to the ablated blunt body problem. Comp. and Fl. 10, 277-294 (1982).

13. Moretti, G.: The choice of a time-dependent technique in gas dynamics. AGARD Lecture Series 48, (11),1-23, 1972.

14. Moretti, G.; Complicated one-dimensional flows. PIBAL Rep. 71-25, 1971 (Pol. Inst. of Brooklyn).

15. Moretti, G.; Three-dimensional, supersonic, steady flows with any number of imbedded shocks. AIAA Paper 74-10, 1974.

1. Report No.	2. Government Accession No.	3. Recipient's Catalog No.
NASA CR-3712		

4. Title and Subtitle	5. Report Date
AN IMPROVED LAMBDA-SCHEME FOR ONE-DIMENSIONAL FLOWS	September 1983
	6. Performing Organization Code

7. Author(s)	8. Performing Organization Report No.
Gino Moretti and Michael T. DiPiano	
	10. Work Unit No.

9. Performing Organization Name and Address	11. Contract or Grant No.
G.M.A.F., Inc. P.O. Box 184 Freeport, NY 11520	NAS1-16946
	13. Type of Report and Period Covered
12. Sponsoring Agency Name and Address National Aeronautics and Space Administration Washington, D.C. 20546	Contractor Report
	14. Sponsoring Agency Code

15. Supplementary Notes

Langley Technical Monitor: James C. Townsend
Final Report

16. Abstract

A code for the calculation of one-dimensional flows is presented, which combines a simple and efficient version of the lambda-scheme with tracking of discontinuities. The latter is needed to identify points where minor departures from the basic integration scheme are applied to prevent infiltration of numerical errors. Such a tracking is obtained via a systematic application of Boolean algebra. It is, therefore, very efficient. Fifteen examples are presented and discussed in detail. The results are exceptionally good. All discontinuities are captured within one mesh interval.

17. Key Words (Suggested by Author(s))	18. Distribution Statement
Computational Fluid Dynamics Supersonic Flow Shock Waves Finite-Difference Methods	Unclassified-Unlimited Subject Category 02

19. Security Classif. (of this report)	20. Security Classif. (of this page)	21. No. of Pages	22. Price*
Unclassified	Unclassified	74	A04

* For sale by the National Technical Information Service, Springfield, Virginia 22161

NASA-Langley, 1983